In presenting the dissertation as a partial fulfillment of the requirements for an advanced degree from the Georgia Institute of Technology, I agree that the Library of the Institute shall make it available for inspection and circulation in accordance with its regulations governing materials of this type. I agree that permission to copy from, or to publish from, this dissertation may be granted by the professor under whose direction it was written, or, in his absence, by the Dean of the Graduate Division when such copying or publication is solely for scholarly purposes and does not involve potential financial gain. It is understood that any copying from, or publication of, this dissertation which involves potential financial gain will not be allowed without written permission.

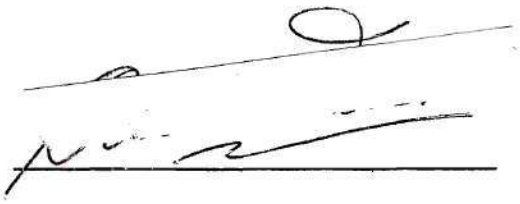

7/25/68

FLAT FLAME BURNER WITH AN OPPOSED NITROGEN-ALUMINUM PARTICLE JET

A THESIS

Presented to

The Faculty of the Graduate Division

by

Clarence Alfred Fisk

In Partial Fulfillment

of the Requirements for the Degree

Master of Science in Mechanical Engineering

Georgia Institute of Technology

March, 1971

FLAT FLAME BURNER WITH AN OPPOSED

NITROGEN-ALUMINUM PARTICLE JET

Approved:

C

Date approved by Chairman: March 11, 1971

ACKNOWLEDGMENTS

The writer expresses his appreciation to Dr. Pandeli Durbetaki, his thesis advisor, for his interest, direction, and constant help in all the development aspects of this thesis.

Dr. C. W. Gorton and A. E. Bergles are due a special note of thanks for their sincere interest and constructive comments as readers.

The help and assistance of Messrs. J. Davis and J. Doyal is also appreciated.

The writer would like to express his gratitude to his wife, Patricia, for her patience, understanding, and encouragement during some trying periods in the development of this thesis.

TABLE OF CONTENTS

TABLE OF CONTENTS (Concluded)

LIST OF TABLES

LIST OF ILLUSTRATIONS

LIST OF ILLUSTRATIONS (Continued)

LIST OF ILLUSTRATIONS (Concluded)

NOMENCLATURE

Symbol	
a	stochiometric coefficient
A/F	air-fuel ratio
b	stochiometric coefficient
d	thermocouple diameter
E	thermocouple emissivity
e	gas emissivity
H	probe height above the burner disc
h	convection heat transfer coefficient
h_f^o	standard enthalpy of formation
h_T^o	enthalpy at 14.7 psia and the temperature T
k	gas thermal conductivity
$\dot{m}$	mass flow rate
N	a number function of the mean temperature, gas conductivity and Reynold's number
n	light chopper revolutions
Q	heat of reaction
q	combined heat lost by radiation and convection
R	universal gas constant
s	true distance between two particle traces
T	absolute temperature
t	temperature, time elapsed between two segments of particle traces

NOMENCLATURE (Concluded)

Symbol

V	gas velocity
$\dot{V}$	volumetric flow
v	particle mean speed
α	gas absorptivity, radiation heat transfer coefficient
ϵ	emissivity
σ	Stephan-Boltzman constant
μ	gas viscosity
ρ	gas density
Φ	combustion completion ratio

Subscripts

c	refers to the thermocouple or to the measured temperature
g	refers to the gas
m	mean
p	refers to the particle
r	refers to radiation
w	refers to the wall

SUMMARY

This work is the continuation of experiments on an existing flat flame burner, which incorporates an opposed nitrogen-aluminum particle jet. This burner was designed and first tested by M. A. Shakill in fulfillment of the requirements for the degree of Master of Science in Mechanical Engineering. The equipment and techniques used by Shakill were altered for a more quantitative evaluation of the behavior and reaction of 50 micrometer diameter aluminum particles (ALCAN M.D. X-85-1). The hot gaseous environment was produced by a pre-mixed methane-air flat flame.

Chromel-alumel thermocouple probes, mounted on a traversing mechanism, were introduced in the hot gases for temperature measurements. The probe was introduced in the flame through a port made in the pyrex glass chimney.

Temperature measurements were made first for an undisturbed flame; then for one with an opposed nitrogen jet. Measurements were then made using the same flame with the opposed nitrogen jet with aluminum particle addition.

The temperature profiles and field of the flame, cooling effect of the nitrogen carrier jet, and temperature variation caused by aluminum particle addition were compared. All measured temperatures were corrected to account for radiation losses.

Aluminum particle reaction was estimated by making an energy bal-

ance, first for the flame with the opposed nitrogen jet and then for one with the opposed gas-particle jet. The percentage of aluminum consumed and particle diameter reduction were calculated.

Still photography was used to estimate particle mean speeds. Particle ignition was evidenced as sharp sudden luminosity of the particle tracks on the photographic plate and by personal observation. Also the occurrence or non-occurrence of particle macroscopic movements, such as spinning and fragmentation were observed.

CHAPTER I

INTRODUCTION

The combustion and burning of metals is poorly understood compared to the combustion of the more conventional fuels. A better understanding of the phenomena involved will permit obtaining higher temperatures from the conventional fuels by the addition of metal particles. The metals have the advantage over other fuels because of their high heats of combustion and intensive light emission. Also a better understanding of the combustion of metal particles should aid in the prevention of metal-dust explosions, as well as in the control and burning of metal particles from industrial exhaust gases.

In the last two decades much has been accomplished in the field of heterogeneous combustion. Most studies have been made with low molecular weight metals, such as: aluminum, beryllium, magnesium, zirconium, and boron. These metals have been investigated for their use in rocket fuels.

The combustion characteristics of spherical metal particles that have been studied by different investigators in the field are metal ignition temperatures, particle burning times, and macroscopic movements in the hot gases.

A. Background

A summary of heterogeneous combustion literature is found in

Shakill's thesis entitled "Design and Preliminary Testing of a Pre-mixed Flat-Flame Burner Incorporating an Opposed Gas Particle Jet" (1). In the present work the principal statements and theories are discussed and Shakill's survey is complemented with recent reports from different investigators.

In the last two decades much has been accomplished in the field of metal combustion. Most studies, both experimental and analytical, refer to the ignition and combustion characteristics of single spherical metal particles or wires. These particles were injected into the environment in the same direction as the flame front. Low molecular weight metals, such as aluminum, beryllium, boron, zirconium, and magnesium were used (2,3 thru 18). The hot gaseous environments were produced by the combustion of hydrocarbons, carbon-monoxide, and hydrogen in air or in an oxygen-argon atmosphere.

Two models have been proposed for the analytical study of the combustion of spherical metal particles; namely the surface burning and the vapor-phase models. In the surface burning model the metal particle is considered to start burning by the slow oxidation of its surface. The oxide formed acts as a protective layer retarding further burning. The oxygen must diffuse through the oxide coating to get to the metal. The metal vapor diffuses toward the oxide layer, thickening and increasing the size of the oxide shell. For the metal to ignite the melting point of the oxide must be reached (2). This correlation between ignition temperature and oxide melting point has been observed in the laboratory, for aluminum particles, by Friedman and Macek (3).

The vapor phase model proposed by T. Brzustowski and I. Glassman (7,8) has a thin homogenous reaction zone characterized by the flame front which surrounds the metal particle. Heat is transferred to the metal particle from the flame front causing the metal to evaporate. The metal vapor diffuses to the reaction zone where it reacts with the oxidizer. The products diffuse from the flame front toward the ambient gases.

R. Bartlett (2) used the surface burning model for his analytical study. The model was used to calculate metal ignition temperature and burning rates. D. K. Kuehl (13) has an analytical study using the vapor-phase model. He assumes two phases for the particle reaction, an ignition phase and a combustion phase. The first phase involves the heating of the particle to some ignition temperature. This is a heat exchange process without any chemical reaction. The second phase is the reaction of the ignited particle with the oxidizer. Again using this model Kuehl has calculated ignition temperatures and particle burning rates.

Photographic methods were employed by some investigators to observe macroscopic particle movements such as spinning, splitting, and fragmentation (3,4,11). The surface burning model explains these phenomena. If the growth of the oxide shell is too fast, due to sudden intense heating, it will burst causing the fragmentation and spiral movement of the metal particle. The vapor-phase model does not explain these phenomena.

A simple criterion for predicting whether surface or vapor-phase

burning will take place was proposed by I. Glassman (10). The flame temperature cannot exceed the boiling point of the oxide; surface burning will occur only if the oxide is more volatile than the metal and vapor-phase burning will occur in the opposite case.

Burning times, particle residence times, and particle mean speeds have been calculated from still photographs and high speed motion pictures (2). The particle residence time is defined as the time it takes the particle to preheat and to ignite in the hot gas. Burning time is the period elapsed from ignition until the particle is consumed. The ignition of the particles is detected on the photographic plate as a sudden sharp increase in luminosity of the particle track.

Particles at different stages of their reaction process were collected on slides, introduced at different positions in the hot gases, for microscopic study by Friedman and Macek (3). They reported that such particle macroscopic movements are affected by the content of free oxygen in the hot ambient gases; the results are not conclusive. Also, it has been observed that particles will not ignite in all air-fuel mixtures. A critical temperature must first be attained.

A most important experimental result by Friedman and Macek (3), that has also been shown analytically, is the dependence of the particle ignition temperature on the particle size. This temperature is proportional to the square of the particle diameter.

Temperature measurements of the gas were to be carried out in the present work; therefore, research was done on the techniques and apparatus used by different investigators. The conventional methods are

thermocouples (shielded and un-shielded), resistance thermometers, suction pyrometers, and radiation pyrometers (3,19,20 thru 26). A most interesting method used by Macek (3) consists of the following: a flat flame burner was designed in which the porous burner disc (flame holder) was water cooled through a copper block. The adiabatic flame temperature was first calculated for the propane-oxygen-nitrogen system at one atmosphere and 300°K initial temperature. An IBM program was used to account for all dissociation equilibria. The heat loss to the burner disc was calculated measuring the temperature rise of the cooling water. This method yields results comparable to those obtained by direct measurements.

M. Fishenden (27) proposed a simple method to calculate the temperature error due to radiation losses from the thermocouple inserted in the hot gases. This method was used to correct all measured temperatures and will be explained in detail in Appendix B of this work.

B. Statement of the Problem

The general purpose of this work was to continue the experiments on the existing flat flame burner, which incorporates an opposed nitrogen-aluminum particle jet. The burner was designed and first tested by Shakill. His goal was to obtain a one-dimensional laminar flat flame using methane as fuel and air as the oxidizer. Aluminum particles, 50 micrometers in diameter, were introduced, in an opposed jet. Nitrogen was used as carrier and particle diluent. Particle reaction was evaluated through temperature measurements and by using photography (1).

Shakill had some difficulties in his preliminary tests with the

burner. For a more quantitative evaluation of particle reaction and behavior, in the present work, it was necessary to introduce some alterations in the equipment and techniques. These will be discussed in detail in Chapter II.

A review of the literature reveals that the temperature needed to ignite a single aluminum particle, traveling in the direction of the flame front, is that of the melting point of the aluminum oxide. The melting point of aluminum oxide is approximately 2300°K (3). In our burner this temperature cannot be reached.

The behavior and reaction of 50 micrometer diameter aluminum particles were to be studied at temperatures below the melting point of the oxide. A cloud of metal particles, using nitrogen as carrier gas and particle diluent, were to be introduced in the reaction zone through an injection nozzle to permit some preheating of the particles.

Particle ignition, mean speeds, and macroscopic movement were to be studied using still photography. Particle mean speeds were to be calculated from the traces on these photographic records. For these measurements and observations the mass flow rates of particles and carrier gas were to be varied for different air-fuel ratios of the flat flame.

The metal particle macroscopic movements were to be observed on the photographic plates as sudden changes in the particle path.

C. Remarks

According to I. Glassman's statement (10), aluminum particles should burn in the vapor-phase system since the oxide is less volatile

than the metal. Macek and Friedman (3) have collected aluminum particles in different stages of their reaction on slides for microscopic studies. They have photographed them and they show aluminum metal surrounded by an oxide shell that increases in size and thickness as the metal is consumed. These findings suggest that aluminum particles react in the surface burning system. Another phenomenon that suggests that aluminum reacts in the surface burning system is the observed particle macroscopic movement, such as spinning and fragmentation (3,4). Discrepancies exist between the two theories.

Most investigators have studied only the behavior of single aluminum particles (10 to 300 micrometers in diameter) traveling in the same direction as the flame front. The ignition temperature reported is approximately 2300°K (3). The present work deals with a cloud of 50 micometer particles injected in an opposed jet, allowing for particle preheating and longer interaction in the hot gaseous media. Particle ignition was observed in flames with temperatures as low as 1200°K (1700°F). The need for more extensive research in the field is very much apparent.

CHAPTER II

INSTRUMENTATION AND EXPERIMENTAL TECHNIQUES

A. Burner and Accessories

The flat flame burner used for this work was designed by Shakill (1). Figure 1 shows schematically the burner with the auxiliary traversing mechanism and temperature measuring probe. Figure 2 is the complete installation and flow diagram.

The burner will be discussed only briefly, since a complete detail is given in Shakill's thesis. The mixing chamber, item 13 in Figure 1, is a steel pipe, 10 inch I.D. and 24 inches long. Six 200 mesh stainless steel screens, 12, at $1\frac{1}{2}$ inches apart from each other are located at the upper end of the cylindrical chamber. The air and methane inlets are located at the bottom of the chamber, 14, 15. The mixing chamber is connected to the burner tube, 17, by a cast aluminum transition piece, 11. The burner tube, made of brass has a 3.28 inch I.D. and is 14.5 inches long.

Near the bottom of the burner tube there is a 30 mesh stainless steel screen. The tube is filled up to $3\frac{1}{2}$ inches from the top with three millimeter diameter glass beads. These are used for further gas mixing and flow calming.

A sintered bronze porous disc, 6, is fixed to the burner tube in a bronze holder ring by three screws. The disc is used as the flame holder and to avoid any flash-back.

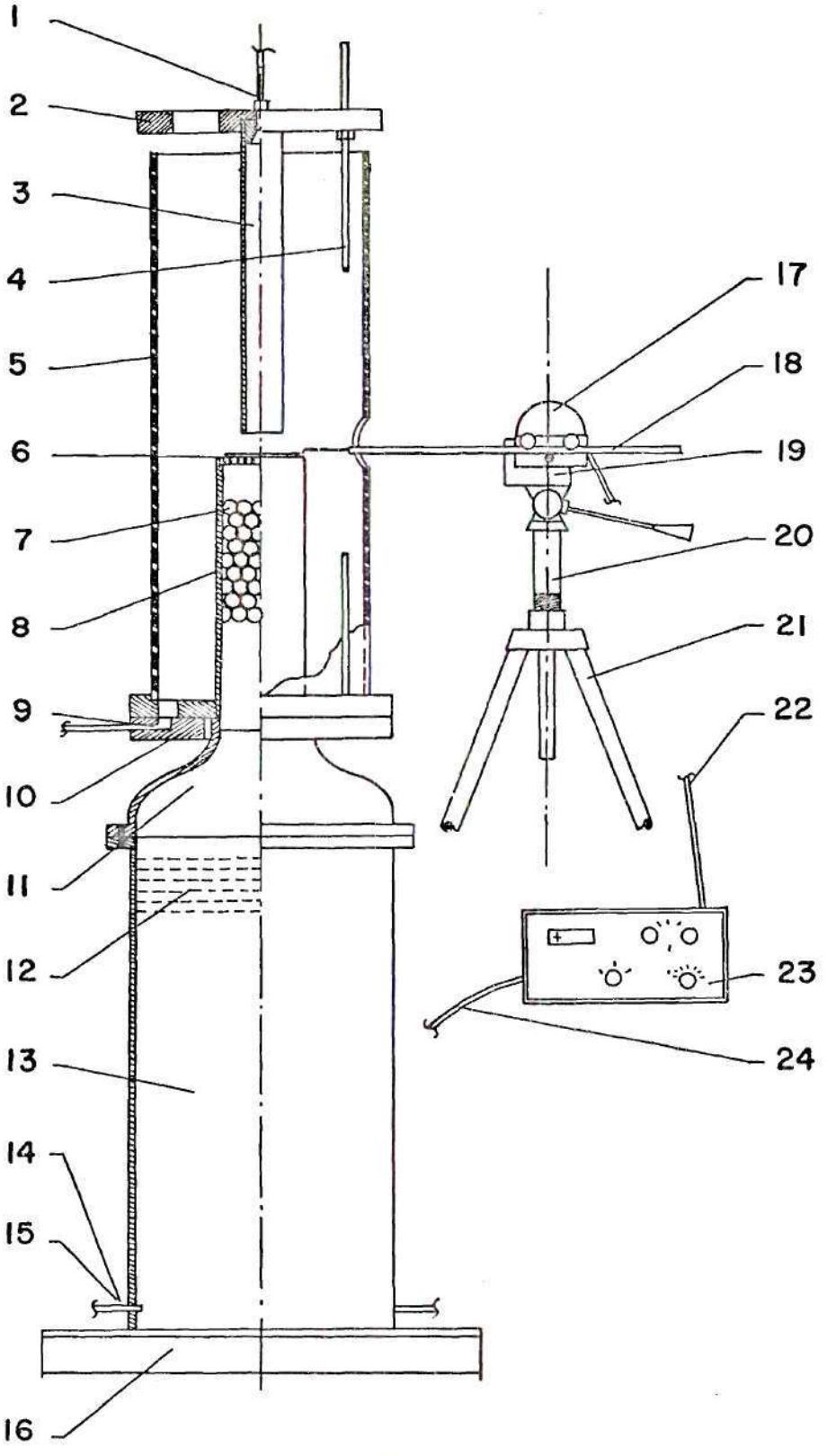

Figure 1. Flat Flame Burner Cross-section & Temperature Probe Traversing Mechanism.

Description of Figure 1

1 $\frac{1}{8}$" aluminum particle and nitrogen carrier inlet

2 injection nozzle supporting ring

3 1" I.D., stainless steel injection nozzle

4 supporting rods (3-3/8" dia. at 120°)

5 6" dia. by 24" long pyrex glass chimney

6 $3\frac{1}{4}$" dia. by $\frac{1}{4}$" thick sintered porous bronze burner disc

7 $3\frac{1}{4}$" dia. by $14\frac{1}{2}$" long brass burner tube

8 3 mm diameter glass beads

9 $4\frac{1}{4}$" cooling nitrogen inlets

10 aluminum supporting table

11 cast aluminum transition piece

12 six 200 mesh stainless steel screens

13 10" dia by 24" long mixing chamber

14 $2\frac{1}{4}$" methane inlets

16 steel carriage

17 stepper motor

18 thermocouple probe

19 stepper motor and probe support

20 height regulating sleeve and nut

21 tripod

22 stepper motor power input

23 DISA sweep unit generator

24 sweep unit input (110V - 60 c/s)

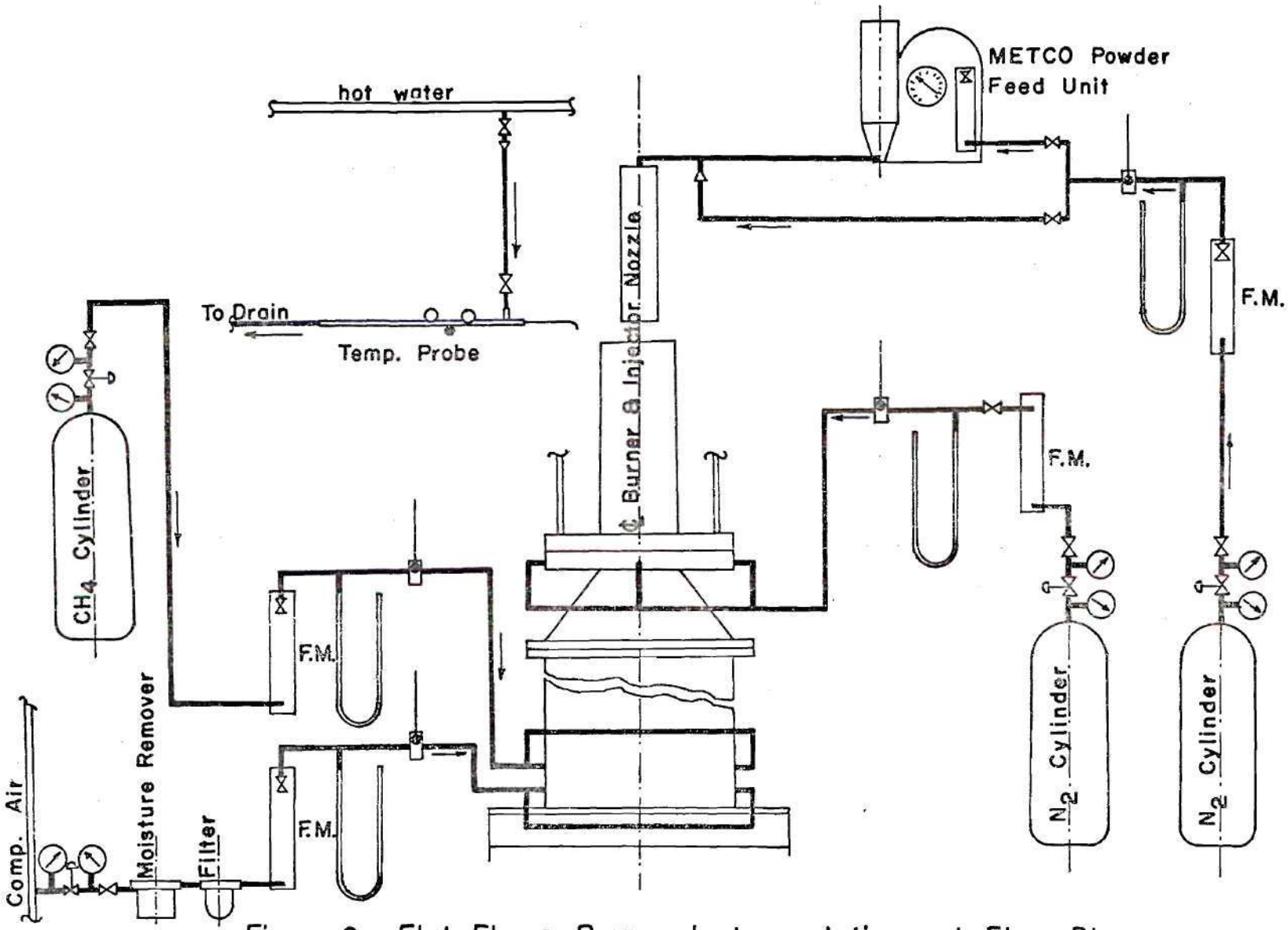

Figure 2. Flat Flame Burner Instrumentation and Flow Diagram

A pyrex glass chimney, 5, six inches I.D. and 24 inches long, encloses the burner tube and particle injection nozzle. It acts as a chimney and avoids any disturbances due to air drafts. The chimney is set on an aluminum supporting disc, 10, that is screwed to the transition piece, 11.

The particle injection nozzle, 3, one inch I.D. and 12 inches long, made of stainless steel, is fitted into a steel ring, 2. The whole structure is fastened to the supporting table by three $\frac{3}{8}$" and 30" long steel rods. The nozzle is used to introduce the aluminum particles in the reaction zone, using nitrogen as carrier gas. The injection nozzle and its supporting ring can be adjusted axially by six $\frac{3}{8}$" leveling nuts.

Figure 2 shows schematically the complete installation and designates the flow of the fluids in the system. Essentially it is the same as the one used by Shakill. Some changes were made; these will be discussed in a later section.

The pre-mixed methane-air flat flame is produced on the upstream side of the porous disc. Methane was supplied in high pressure cylinders. Air for the combustible mixture was furnished from an 80-125 psig main line. A pressure regulator is installed on each line for pressure reduction and initial flow control. The flow was measured by variable area flowmeters furnished with needle valves on the upstream side of the meters. Methane pressure was read on a 24 inch water manometer while the air pressure was read on a 50 inch mercury manometer. The temperature of air and methane was measured by mercury thermometers at the downstream side of the flowmeters.

Methane and air, after flowing through their respective controls and measuring instruments, were directed to the bottom of the burner mixing chamber, item 13 of Figure 1.

The particle carrier gas was also supplied in high pressure cylinders. The control and measuring devices consist of a two-stage pressure regulator, a flowmeter, a 50 inch mercury manometer, and a mercury thermometer.

The carrier nitrogen was split into two streams. One stream was directed to the powder feeder to dilute the aluminum particles, while the other stream by-passed the feeder. The two streams were reunited at the discharge nozzle of the powder feeder unit.

The powder feeder unit (Metco Type 3MP) is a positive metering device; it delivers particles at a controlled adjustable rate. The feeder has a rotating bucket wheel that picks up powder and delivers it to a mixing chamber. The speed of the wheel can be varied; the amount of particles delivered is proportional to the wheel speed. Downstream of the wheel the nitrogen picks up particles and takes them to the discharge nozzle.

Shakill's feed line to the burner injection nozzle consisted of a $\frac{3}{16}$" line with a small electric vibrator attached to it to prevent the accumulation of particles.

Aluminum powder (Alcon Metal Inc. grade MD-X85-1) was the only material used in this experimental study consisting of spherical solid metal particles with an average diameter of 50 micrometers.

This installation presented problems in Shakill's tests: high

mass flow rates of particles being dumped in the reaction zone resulting in excessive accumulation on the burner disc and a secondary reaction zone at the periphery of the flat flame. A leaner mixture was found at the flame edges due to the additional oxygen from the air that circulated between the burner tube and the glass chimney.

A uniform mass flow rate of particles could only be sustained during short periods; hence there was little time for accurate temperature measurements.

It was necessary to introduce some alterations to this set-up to correct these problems. They can be divided into three parts: alterations to the burner, alterations to the powder feeder unit, and alterations to the feed lines.

B. Alterations to the Burner

In an attempt to eliminate the secondary reaction zone at the periphery of the flame, nitrogen was circulated between the burner tube and the chimney. The supporting table, 10, was redesigned with addition of an aluminum blind flange with four $\frac{1}{8}$" inlets for the nitrogen. The nitrogen flow also helped cool the transition piece, 11, reducing the heat conducted through the burner tube. The cooling nitrogen was supplied in high pressure cylinders. The control and measuring devices consisted of a two-stage pressure regulator, a variable area flowmeter, a mercury manometer, and a thermometer.

In the later tests it was found that the cooling nitrogen flow distorted the particle tracks and temperature field, as will be discussed in the next chapter. Better results were obtained with the original set-up,

where there was no cooling nitrogen flow and the air simply circulated by free convection.

A two-inch diameter port hole was made in the glass chimney at the height of the burner disc. Temperature probes were introduced through the port hole into the reaction zone. A cerofelt diaphragm was securely taped to the opening to avoid any air drafts.

Additional fuel and air inlets were made in the burner mixing chamber for better air-fuel mixing.

C. Alterations to the Powder Feeder Unit

This unit has a particle feed rate that is too high for the type of experiments being performed. This rate of particles was even higher when the bucket wheel was turning.

Shakill had replaced the bucket wheel supplied by the manufacturer for one with smaller buckets. He reduced the particle feed line from $\frac{1}{4}$" to $\frac{3}{16}$" and also attached an electric vibrator to it upstream from the particle injection nozzle.

In our experiments more modifications were necessary since the preliminary installation had not solved the accumulation and particle dumping problems. The feeder has a discharge nozzle, supplied by the manufacturer, which has a tapered discharge hole starting at $\frac{1}{4}$" and reducing to $\frac{3}{32}$"; it also has a $\frac{1}{4}$" threaded line connection. The two major alterations made were a) the tapered discharge hole was changed to a $\frac{3}{32}$" straight hole and a $\frac{1}{8}$" line connection was provided, and b) the feed line was changed to a $\frac{1}{8}$" copper tube. The redesigned discharge nozzle is shown in Figure 3.

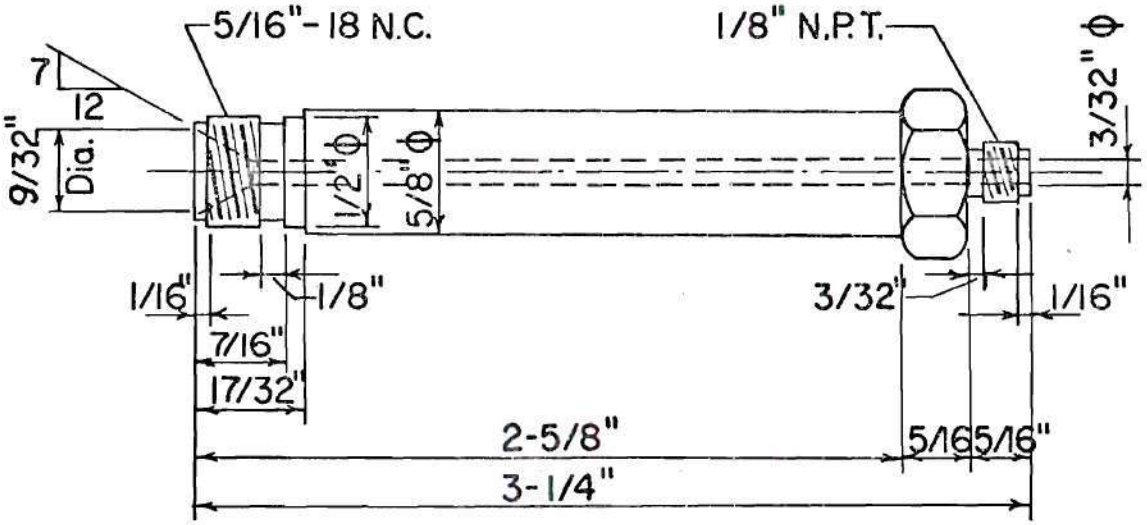

Figure 3. Stainless Steel Powder Feeder Discharge Nozzle.

The powder feeder was relocated to the right of the burner on a table two feet above the burner disc. With this arrangement the particles would not flow against gravity at any point in the feed lines. The new position of the powder feeder made it possible to shorten the feed lines.

In addition to the $\frac{3}{16}$" feed line, Shakill's set-up provided a $\frac{1}{4}$" by-pass connection at a point near the powder feeder discharge nozzle. This by-pass connection was moved to a point directly upstream from the particle injection nozzle (see Figure 2). No electric vibrator was used in the present experiments. A sufficiently uniform particle flow was obtained as a result of these modifications.

In later tests it was observed that, in order to achieve a higher particle mass flow than that used during the initial phases of this experimentation, an excessively high flow rate of carrier gas was required. The cooling effect of this nitrogen on the flat flame disguised any temperature variations produced by particle reaction. The powder feeder bucket wheel was then removed. This provided more contact area between the carrier gas and the particles in the powder feeder and as a consequence the particle density in the carrier gas was substantially increased. With these refinements in the powder feeder and feed line, the burner could be operated without particle accumulation for periods of two to three hours.

After long burner operation the transition piece overheated due to heat conduction through the burner tube. An electric fan was installed to force air against the outside of the transition piece.

A Wilkerson (Model 4001-2) moisture remover was installed down-

stream from the pressure regulator valve on the air line. No attempts were made to remove moisture from the other gases. The moisture content in the bottled gases may be considered to be insignificant.

D. Alterations to the Techniques Used

1. Temperature

Shakill measured the temperature of the hot gases generated by the flat flame with Chromel-Alumel thermocouples (Leeds and Northrup Co. gage 28). A group of four thermocouples were supported on a rod and installed so that all of them had their junctions at the same horizontal level. These thermocouples were used to measure the flat flame temperature in the absence of metal particle injection. Only one potentiometer was used, a thermocouple selector switch was installed between the thermocouples and the measuring instrument.

When the burner was operating with particle injection, Shakill observed that the multiple thermocouple arrangement produced excessive disturbances in the reaction zone and in the reacting metal particles. In this case only one thermocouple was used. The hot gas temperatures above the burner as well as in the flame were measured by this single thermocouple. Reproducibility of temperature measurements is difficult with this method in as much as a slight variation in position of the thermocouple functions will produce measurement differences of up to 100°F.

In these tests the port hole in the glass chimney permitted the introduction of temperature probes into the reaction zone. The temperature probe consists of a $\frac{5}{16}$" diameter steel tube 24 inches long. A $\frac{1}{8}$",

$4\frac{1}{2}$" long double hole alumina spaghetti was attached to one end of the tube. Chromel-alumel thermocouple wire (Leeds and Northrup Co. gage 28) was introduced through the holes in the alumina spaghetti to form the hot junction. The probe was made to traverse over the burner disc using a DISA traversing mechanism. The probe, shown in Figure 4, was water cooled to protect the stepper motor from the heat conducted through the probe.

The traversing mechanism consists of two major components: the DISA sweep drive unit, item 23 in Figure 1, and the external stepper motor, 17. The drive unit is a variable DC generator; it contains all the controls and switches for foward and backward movements of the probe. It is electrically connected to the external stepper motor.

The stepper motor and probe are mounted on a tripod in front of the port hole in the glass chimney. The tripod was set on a table and fixed to a wooden base to avoid any accidental movements. The sweep unit has a three digit mechanical counter allowing for repeatability of stops in the traversing path. The height of the probe can be regulated by a specially designed sleeve and nut incorporated in the tripod assembly (item 20 in Figure 1).

With this mechanism the temperature of the flame and hot gases was measured at as many points as necessary along the burner disc diameter and at different planes parallel to and above the flat flame.

The glass wall temperature was measured with a chromel-alumel thermocouple, gage 28, fixed securely to the wall.

The ice-point was used as a reference temperature and the reference

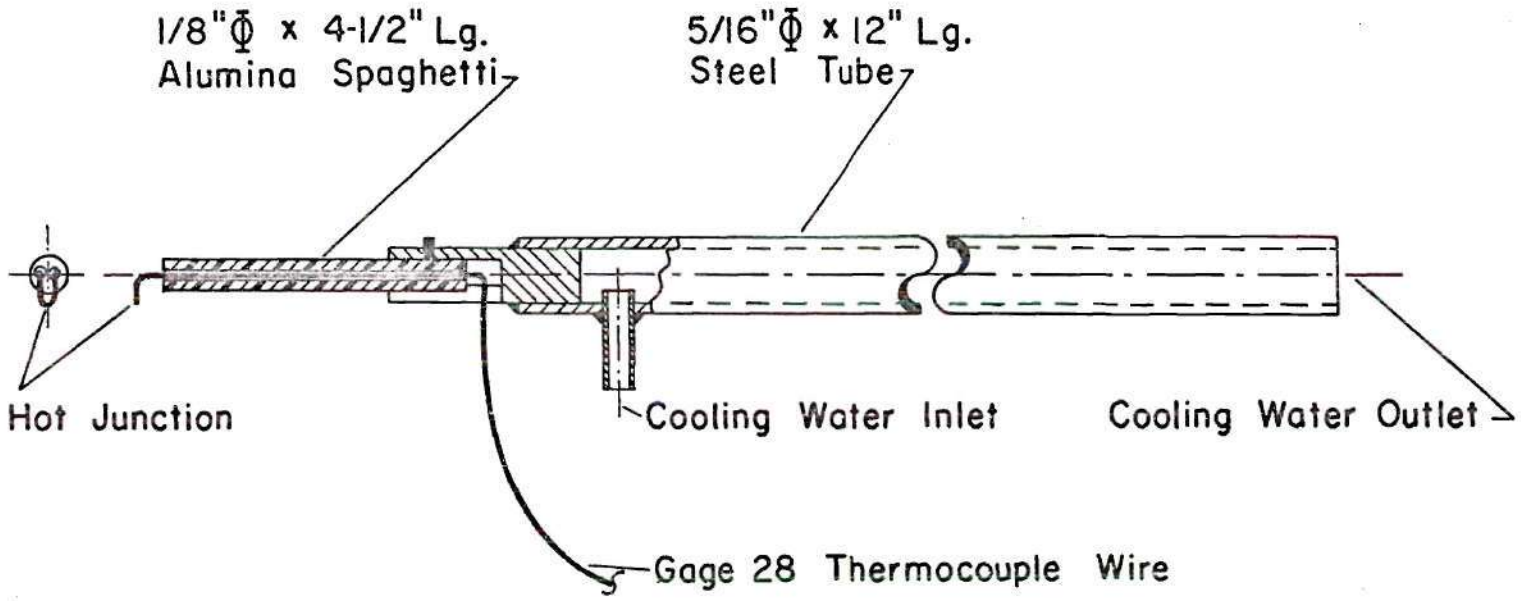

Figure 4. Water Cooled Temperature Probe.

junction was inserted in an ice bath for this purpose. A Leeds and Northrup potentiometer was employed to measure junction emf for the thermocouples and the readings were converted to thermometric degrees using appropriate conversion tables.

2. Still Photography

The only photography used by Shakill was to show reacting particle paths at different particle mass flow rates.

In this work a Speed Graphic 45 Camera with 135 mm, f 4.7 OPTAR lens was used. The objective was to estimate the reacting particles' mean speeds.

A six inch diameter variable slit light chopper driven by a Bodine motor (115 AC/DC, 5000 rpm, 1/100 HP) was mounted on a triangular rail in front of the camera lens. This chopper is generally used for spectroscopic studies and it provides two variable size openings on the disc.

For our work the disc was set to have openings as segments of a ring with $3\frac{1}{2}$ inches inside diameter, $5\frac{1}{2}$ inches outside diameter and an angle of 45 degrees.

The revolutions of the light chopper were controlled by a rheostat. A magnetic pick-up transducer (Electro Products Model 3045A) together with a Hewlett-Packard electronic counter (Model 5233L) were used to record the revolutions of the chopper.

A 20-gage wire was fixed to the burner tube with a steel brace. The wire was made to project $\frac{1}{2}$ inch from the top of the burner disc. It was used to calculate the photographic scale when exposed on the photo-

graphic plate.

In the initial stage of the photographic records, Polaroid black and white film, 3000 ASA, Type 47 ($3\frac{1}{4}$" X $4\frac{1}{4}$") was used. For the main part of the work, where the particle mean speeds were estimated, Kodak TRI-X Ortho, TRI-X Pan, and Royal-X Pan films (4" X 5") were used.

CHAPTER III

PROCEDURE

A. Temperature Measurements

To measure the temperature in the reaction zone, Shakill initially fixed four chromel-alumel thermocouples on a support and adjusted the hot junctions to be in the same horizontal plane. Temperature measurements were obtained when steady-state conditions were reached in the reaction zone, using a thermocouple selector and a potentiometer. For subsequent measurements a single thermocouple was employed.

In the present work the thermometric recordings were achieved through the use of the temperature probe and traversing mechanism described in the preceding chapter. Before lighting the burner, the probe was adjusted both in height and horizontal position relative to the burner disc. For this the glass chimney was first removed. The probe was made to traverse over the burner disc, checking the height and direction of its path. Once the probe was adjusted, the counter on the DISA generator was set so that the zero mark appeared when the hot junction of the thermocouple coincided with the burner axis. The probe was extracted and the glass chimney was replaced in position.

Air was first allowed to flow into the system by opening the valve on the pressure regulator. A total pressure of 40 psig was set with the pressure regulator. The desired mass flow rate of air was obtained with

the needle valve on the air flowmeter. Methane was then allowed in the system by opening the cylinder main valve. The total pressure was set to 10 psig with the pressure regulating valve. The desired methane mass flow rate was set with the needle valve on the methane flowmeter.

The mixture was lit above the burner disc using a spark generated by a hand cranked magneto. The system was allowed to reach steady state conditions before any measurements were made.

The experimental investigation was divided into three distinct phases: a) undisturbed flat flame, b) the flat flame with an opposed nitrogen-aluminum particle jet, and c) the flat flame with only the opposed nitrogen jet.

For the first phase the particle injection nozzle was removed from the system, the thermocouple probe was introduced in the reaction zone, and the height of the hot junction was adjusted by rotating the probe to the point where a maximum millivolt reading recorded on the potentiometer. The temperature corresponding to this reading was found to be in a plane directly above the lower edge of the flame's luminous zone. Measurements were made at points along the diameter of the burner disc at intervals of 50 divisions on the sweep unit counter (approximately $\frac{1}{8}$ inch apart). Once the readings were completed for one plane of the flame, the height of the hot junction was changed with the fine threaded nut and sleeve on the tripod. Thus, measurements were made in horizontal planes $\frac{1}{16}$, $\frac{1}{8}$, $\frac{1}{4}$, $\frac{3}{8}$, $\frac{1}{2}$, $\frac{3}{4}$, 1, $1\frac{1}{2}$, and $1\frac{3}{4}$ inches above the burner disc. For a few initial runs, measurements were also obtained at $\frac{1}{32}$, $\frac{3}{16}$, $\frac{5}{8}$, $1\frac{1}{4}$, and 2 inches above the burner disc.

For the second phase of experimentation, the particle injection nozzle was set in place and the carrier gas-particle flow lines were connected. The nozzle was adjusted first for a desired height of its edge above the burner disc and then for positioning the nozzle axis normal to the burner disc. These adjustments were carried out with the $\frac{3}{8}$ inch nuts on the steel rods supporting the nozzle ring, item 2 of Figure 1. A very low mass flow of carrier nitrogen was set to a value between 0.2 to 1.0 pounds per hour. Part of this flow was directed through the particle feeder and the other part by-passed the feeder to dilute the aluminum particle flow at a point upstream from the injection nozzle. The desired mass flow rate of particles was obtained by regulating the total flow of nitrogen carrier either with the by-pass valve or the needle valve on the powder feeder flowmeter.

The mass flow rate of particles injected was determined by capturing them in a special bottle trap and weighing. The particles were collected in the trap as the flow was allowed to run for a period of 20 minutes. The bottle and particles were weighed on a C. B. Chain-o-matic scale (10^{-4} grams sensitivity). This process was carried out at the beginning and at the end of each test with particle injection and an average mass flow of particles was determined by using the mean of the two weighings.

The temperature measurements were made at the same points and planes above the burner disc as were made for the undisturbed flame.

For the last phase the powder feeder was completely by-passed and only nitrogen was directed into the flame through the nozzle. The nitrogen

flow was set for the same value used in each test of the second phase. This was done to study the cooling effect of the nitrogen jet on the flame. Temperature measurements were then made at the same points and planes above the burner disc as were made for the other two phases.

All these temperatures had to be corrected for radiation losses; the temperature of the pyrex wall was needed for these corrections. A chromel-alumel thermocouple was securely taped on the pyrex wall at $\frac{1}{4}$ inch above the burner disc plane.

The same procedure outlined above was repeated for flames having different combustion completion ratios, different mass flows of aluminum particles, and different mass flows of carrier gas.

B. Still Photography

As discussed in the previous chapter, a Speed Graphic camera was set on a triangular rail normal to the axis of the burner. The light chopper was located between the camera and the burner. The burner was lit and a low mass flow of metal particles was injected into the reaction zone.

For the initial phase of the photographic record, the Speed Graphic camera was used with the Polaroid back to establish the usable range of chopper revolutions as well as camera exposure and aperture setting.

It was thus determined that, with 3000 to 4000 revolutions of the chopper and 10 to 30 seconds exposure time with full camera aperture, a satisfactory record of the interrupted particle path could be achieved. The particle mean speeds can be calculated from these photographs, the

time elapsed between particle traces was known from the light chopper revolutions. The distance between traces was measured directly from the photographs using a pointed compass and micrometer. The scale of each photograph was established from the $\frac{1}{2}$ inch long wire also exposed on the photographic film.

CHAPTER IV

RESULTS

The primary results of this investigation are the estimated percentages of aluminum particle consumption and the calculated mean speeds of particles. The former was achieved through the use of thermometric measurements and an energy balance in the reaction zone; particle mean speeds were determined from the photographic records. A more detailed analysis and discussion of these important results will be carried out in subsequent parts of this chapter.

As was discussed in the preceding chapter, the experimental investigation was divided into three distinct phases: a) the undisturbed flat flame, b) the flat flame with an opposed nitrogen-aluminum particle jet, and c) the flat flame with only nitrogen flow in the opposed jet (no aluminum particle injection).

Table 1 represents a summary of the air-fuel ratios and particle mass flow rates used in this experimental investigation. It is intended to serve as a guide in the discussion of the results that will follow. At the same time, the table includes some measured and calculated values such as flame velocity, maximum reaction zone temperature, and maximum temperature difference, comparing the case with only nitrogen in the opposed jet and the case with the particle-nitrogen jet.

Table 1. Summary of Pertinent Results

Φ	A/F	Flame Velocity		Mass Flow		Reaction Zone Mean Temperature		Maximum Temperature Variation*	
	g Air/g Fuel	in/s	cm/s	Al g/h	N_2 g/h	°F	°K	°F	°K
.914	18.75	2.18	5.56	9.83	475.8	1850	1281	+364	+203
.788	21.78	3.84	9.74	8.41	186.3	1925	1324	+100	+ 56
.720	23.80	2.67	6.78	10.29	475.8	1756	1232	+159	+ 89
.720	23.80	2.67	6.78	7.98	475.8	1756	1232	+135	+ 75
.608	28.32	3.23	8.22	7.82	475.8	1727	1212	- 80	- 44
.556	30.85	3.52	8.93	8.56	475.8	1747	1225	-154	- 86

*Maximum temperature difference detected between the flame with the opposed nitrogen-particle jet and the flame with the opposed nitrogen jet.

A. Thermometric Results

The reaction zone temperature is defined here as the maximum temperature measured directly above the lower edge of the luminous zone in the flame. This temperature is presented in Table 1 for flames with different air-fuel ratios. Figure 5 is a plot of this temperature for undisturbed flat flames and corrected for radiation losses. This temperature depends not only on the combustion completion ratio, Φ, but also on the gas velocity calculated from the combined air-fuel volumetric flow. It was observed that this temperature was located at a higher plane above the burner disc for those flames having the higher gas velocity.

It can be observed that a flame with Φ = .788 and a velocity of 9.74 cm/sec has a higher mean reaction zone temperature than a richer flame with Φ = .914 and a velocity of 5.56 cm/sec. This is observed also for the cases where Φ = .556 and Φ = .608.

Temperature measurements were made for each phase of the experimental investigation at fixed combustion completion ratios and combined mass flow rates of air and methane, at different horizontal planes above the burner disc. The three temperature profiles were plotted on the same graph for comparative display, and they are useful in indicating the temperature field of the undisturbed flame, the cooling effect on the flame caused by the opposed nitrogen jet, and the temperature variation due to aluminum particle addition. Examples of such plots are shown in Figures 6, 7, 8, 9, and 10. The remainder on these are included in the Appendix.

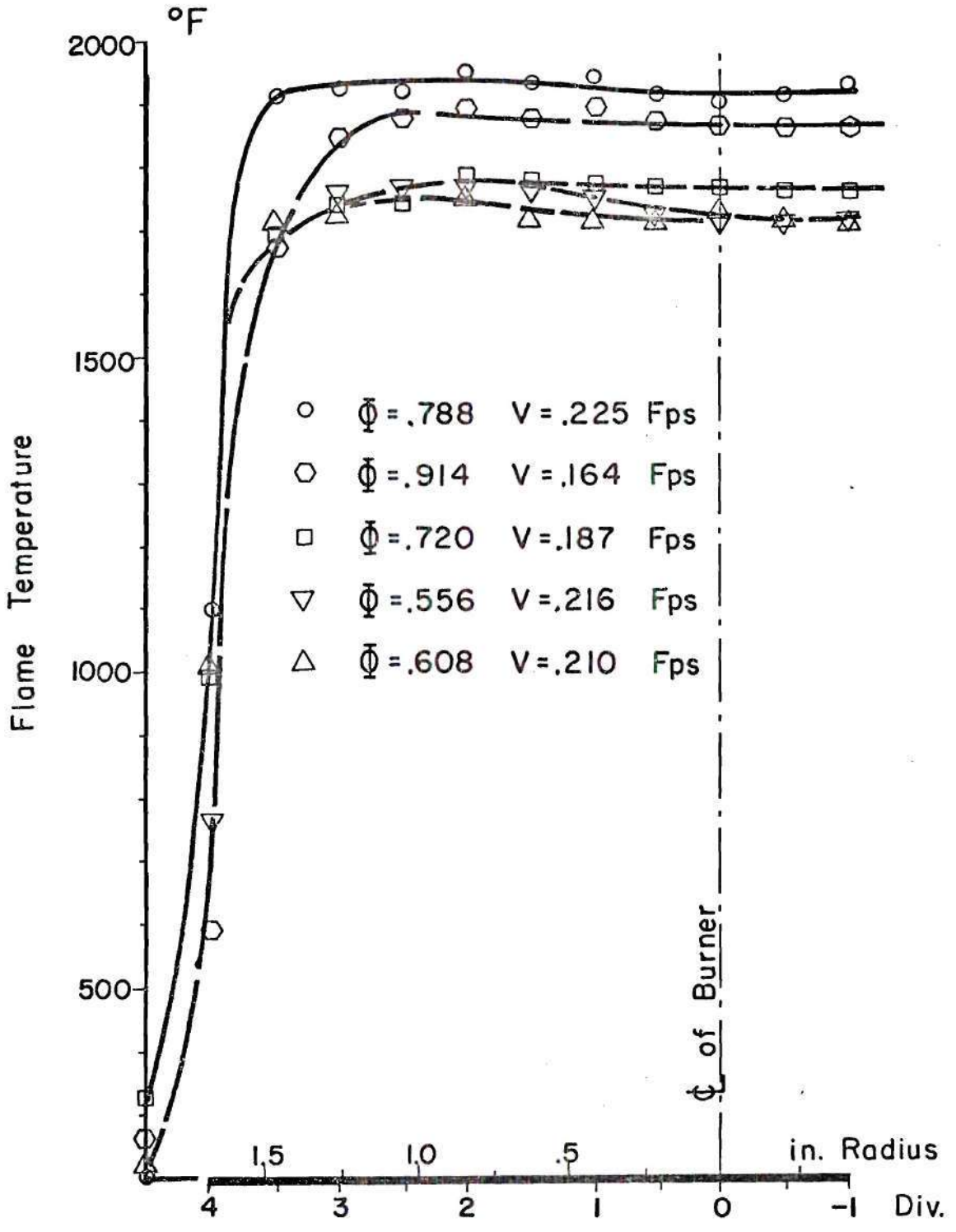

Figure 5. Reaction Zone Flame Temperatures

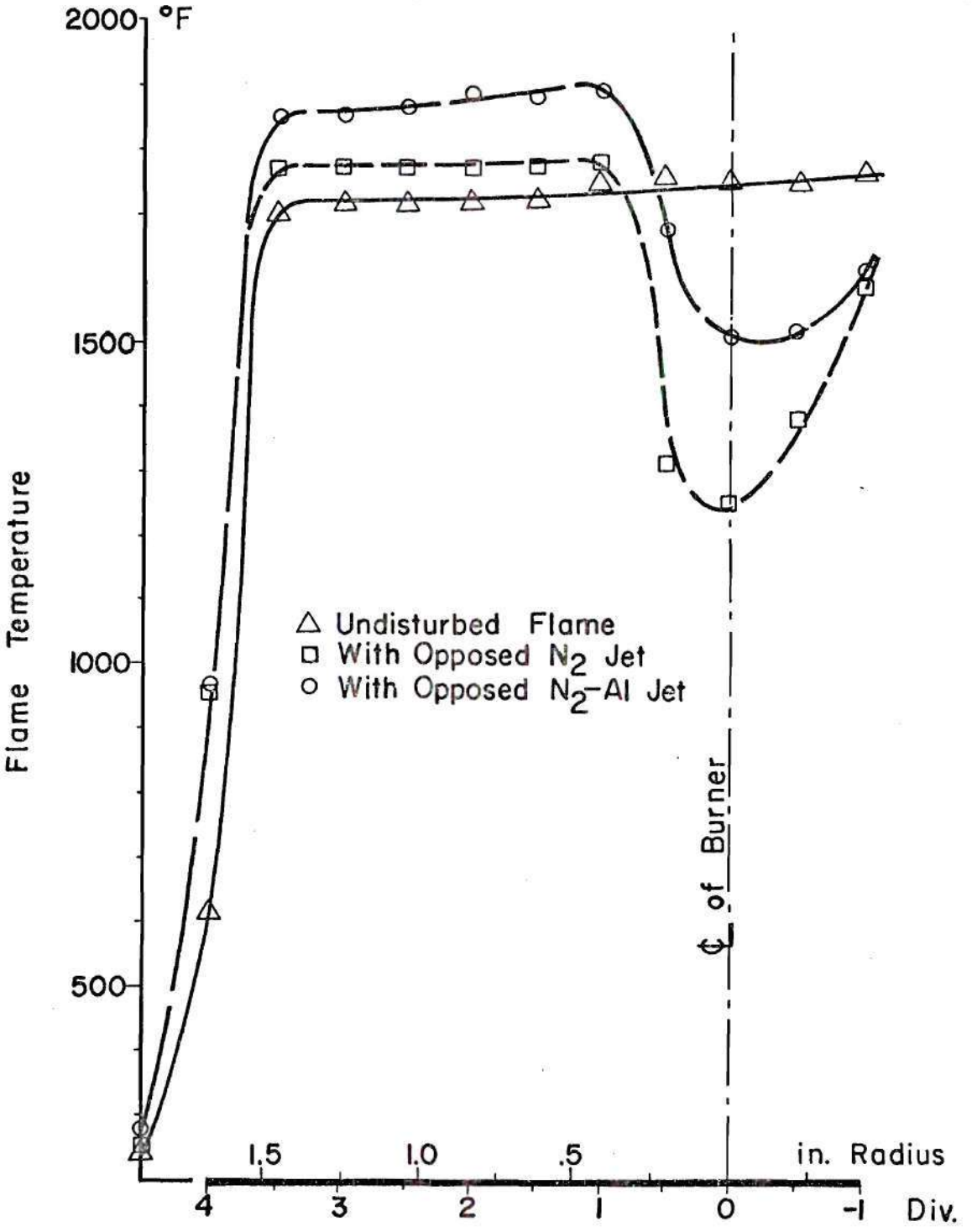

Figure 6. Temperature Profiles. $\Phi = .914$, $\dot{m}_{N2} = 475.8$ Grph, $\dot{m}_{Al} = 9.83$ Grph, V = .164 Fps, H = 1/16 in.

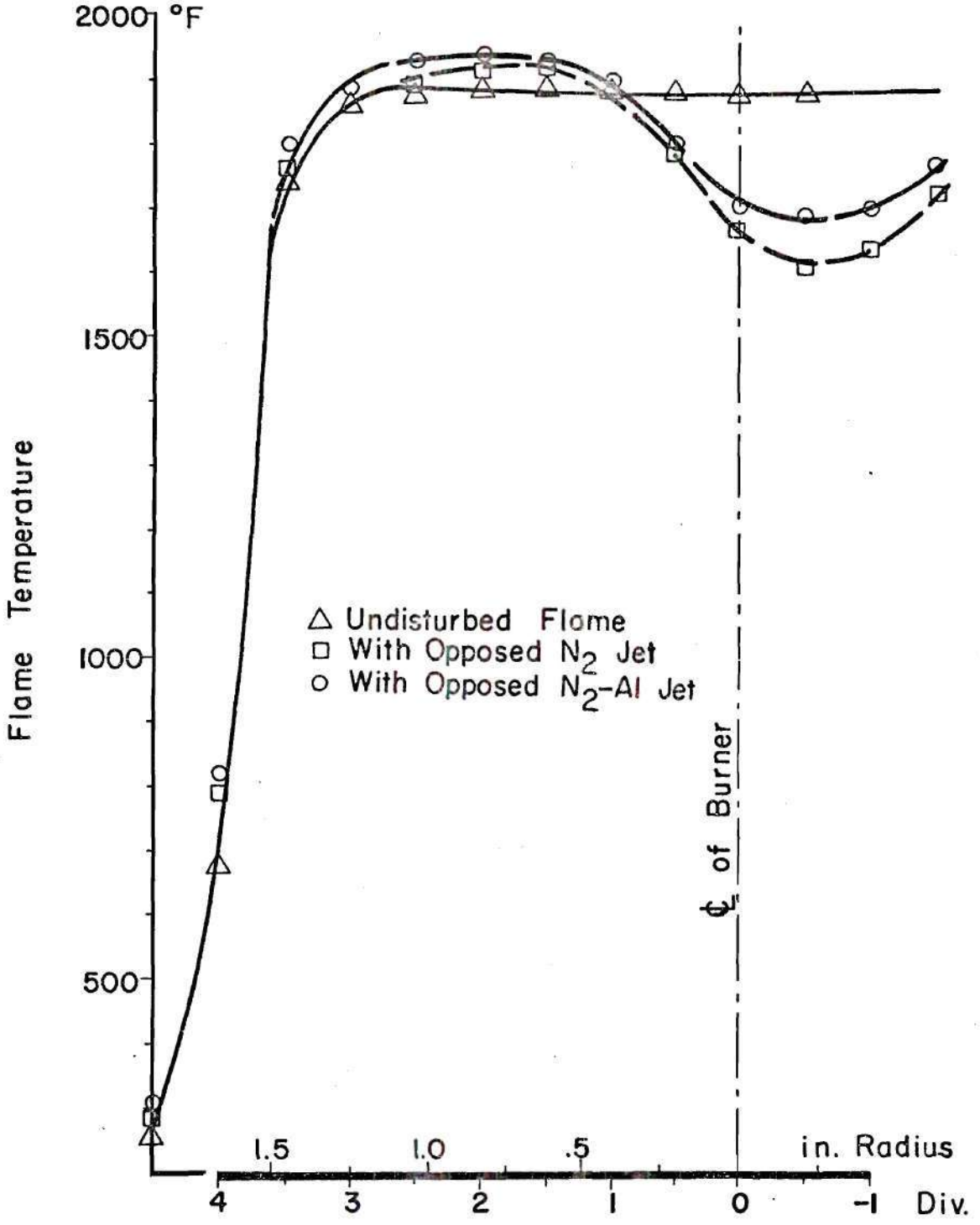

Figure 7. Temperature Profiles. $\bar{\Phi}$ = .788, $\dot{m}_{N2}$ = 186.9 Grph, $\dot{m}_{Al}$ = 8.41 Grph, V = .225 Fps, H = 1/4 in.

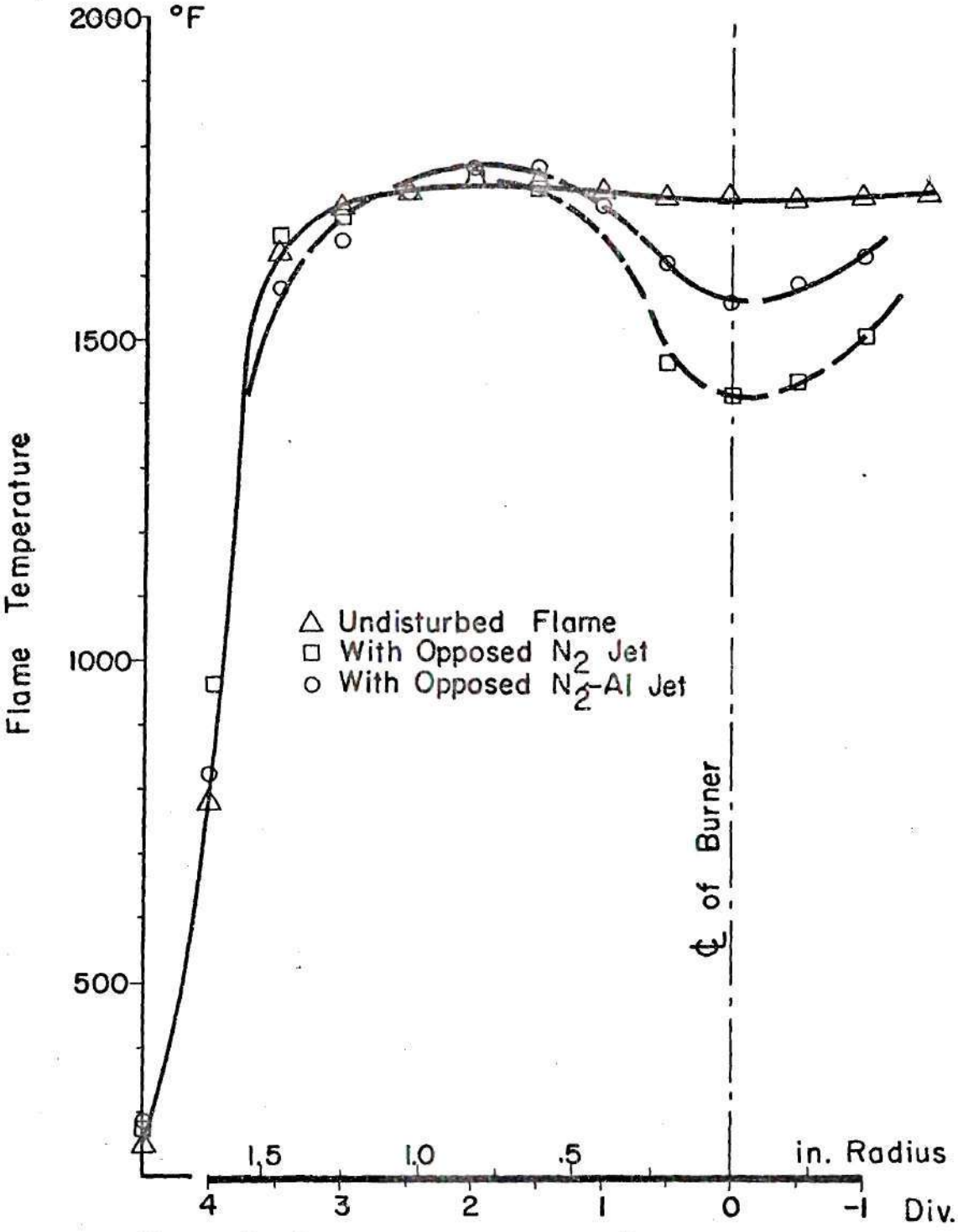

Figure 8. Temperature Profiles. $\Phi = .720$, $\dot{m}_{N2} = 475.6$ Grph, $\dot{m}_{Al} = 10.29$ Grph, V = .185 Fps, H = 1/8 in.

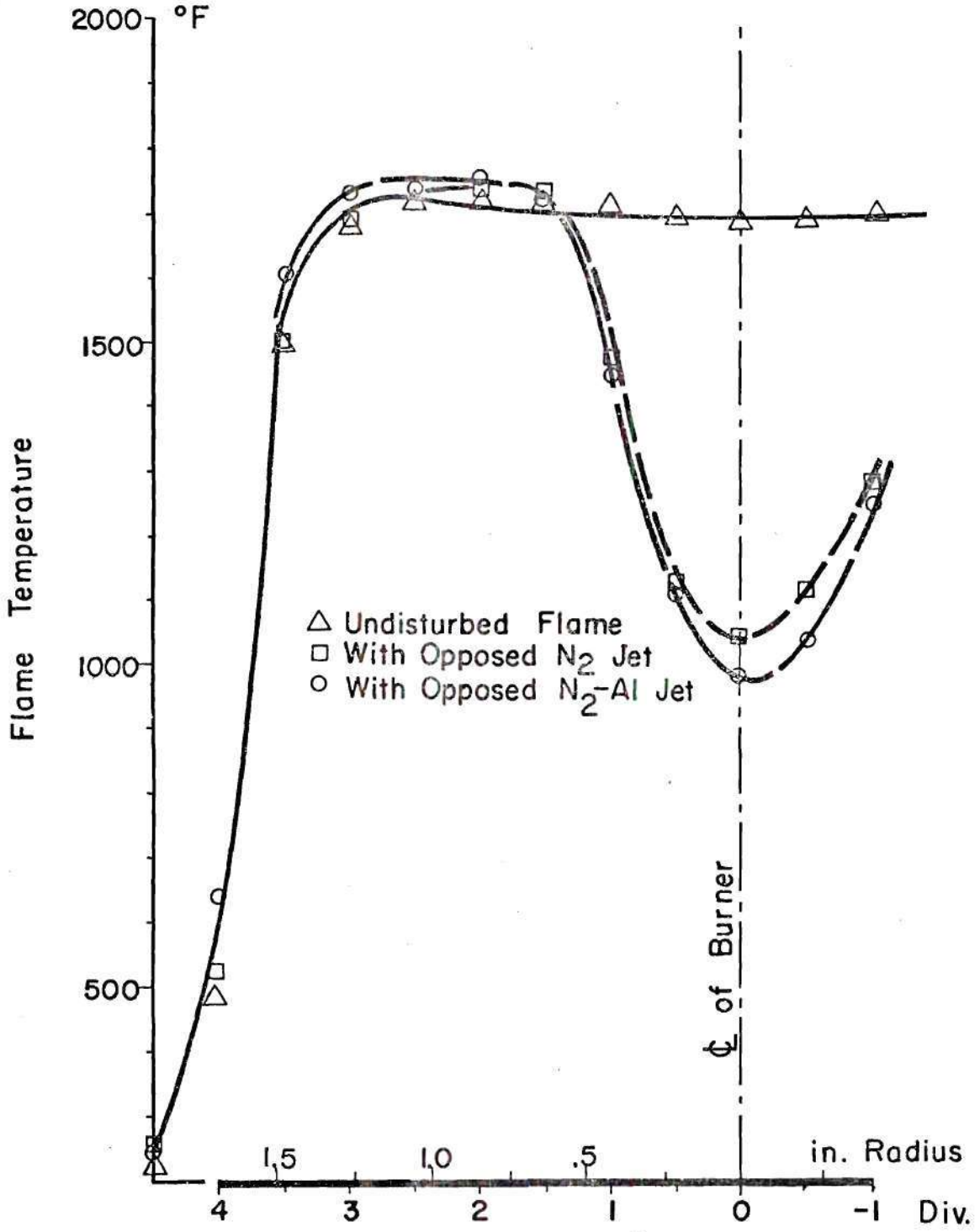

Figure 9. Temperature Profiles. $\Phi = .608$, $\dot{m}_{N2} = 475.8$ Grph, $\dot{m}_{Al} = 7.82$ Grph, V = .210 Fps, H = 1/4 in.

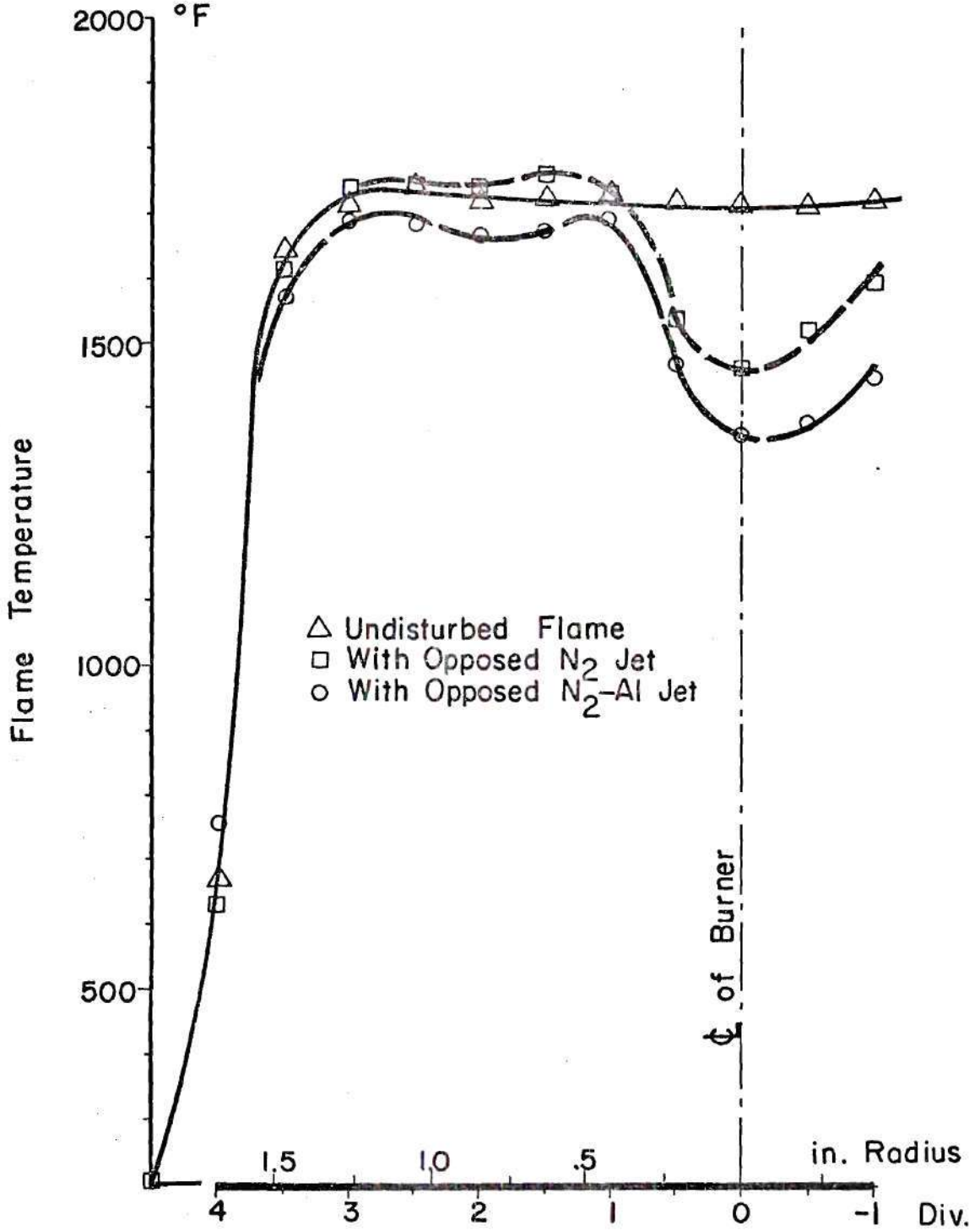

Figure 10. Temperature Profiles. $\bar{\Phi}$= .556, $\dot{m}_{N2}$=475.8 Grph, $\dot{m}_{Al}$=8.56 Grph, V=.216 Fps, H=1/16 in.

A definite temperature rise due to metal particle injection in the reaction zone was detected for flames having combustion completion ratios between .91 and .72. The maximum temperature rise detected was 203°K for a flame with Φ = .91, an aluminum particle flow of 9.83 g/h and with 475.8 g/h of nitrogen carrier flow. The cold nitrogen and particles from the jet entering the region above the burner disc will absorb energy from the hot gases; aluminum particles react with an exothermic reaction. It is apparent that, for this group of air-fuel ratios, the energy released by the particle reaction exceeds the energy absorbed by the combined nitrogen-particle mass flow. The maximum temperature rise was generally found directly under the injection nozzle; lower rises were observed toward the edges of the burner disc. This may indicate that the larger portion of the aluminum particle consumption occurs in this region. The temperature rise detected was found to exist in planes ranging from $\frac{1}{16}$ inch to $1\frac{3}{4}$ inches above the burner disc. A temperature decrease or no change was detected at higher planes.

A temperature decrease was observed when aluminum particles were added to flames with combustion completion ratios of .608 and lower. Figures 9 and 10 display examples of such measurements where a temperature decrease was detected; other examples are presented in the Appendix. The maximum temperature drop detected in these cases varied between 35 and 90°K. In this group of air-fuel ratios it is apparent that the energy released by particle reaction did not exceed the energy absorbed by the combined nitrogen-particle flow.

Although there was a temperature decrease in the group of experiments with combustion completion ratios below .608, it was observed that

some particles displayed tracks with a higher luminosity than others. This may be interpreted that even in these cooler flames some ignition occurs. For the richer flames (Φ = .91 to .72) ignition of the metal particles was observed all around the injection nozzle and in substantially greater numbers. Tracks of ignited particles were captured on photographic plates, examples of which are shown in Figures 11 and 12. Others are included in the Appendix.

In these experiments an inversion point temperature of about 1220°K was determined above which the aluminum reaction causes the mean temperature in the reaction zone to rise and below which the temperature will drop when particles are injected in the reaction zone.

The temperature profiles taken at different planes above the burner disc were used to construct isothermal curves. Figure 13 displays the isotherms for an undisturbed flame with a combustion completion ratio of .788. Correspondingly Figure 14 represents the isothermals of the same flame and a nitrogen flow of 607 g/h. The same experimental conditions were carried through for Figure 15 except that an aluminum mass flow of 3.15 g/h was added to the jet flow.

A superposition of the last two figures is shown in Figure 16. It displays the entire region where temperature increase was detected. In this figure the dashed lines correspond to the isotherms of the flame with the opposed nitrogen jet only.

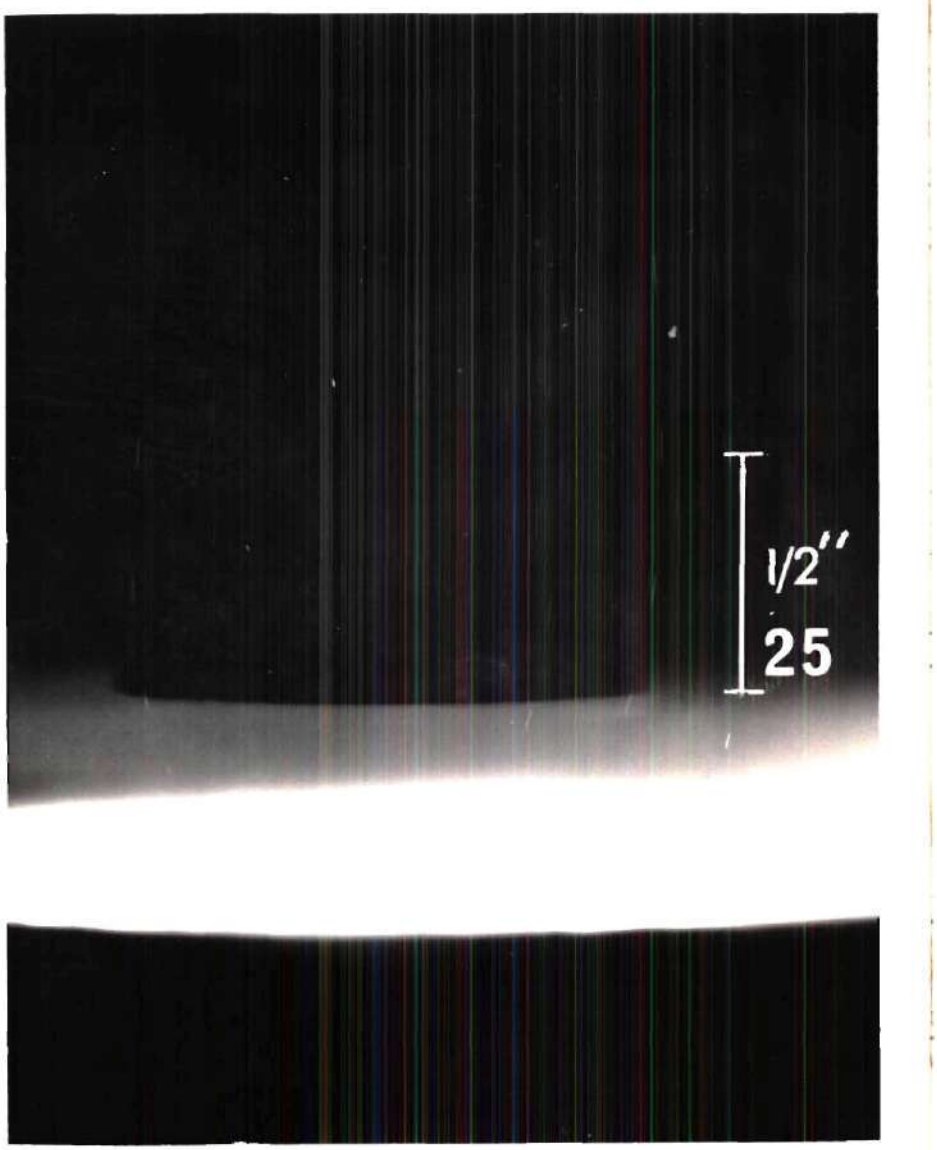

Figure 11. Particle Traces in a Flame with Φ = .788 (Kodal Royal-X Pan, f 4.7, Exposure 10 sec, Chopper Revolutions 4040)

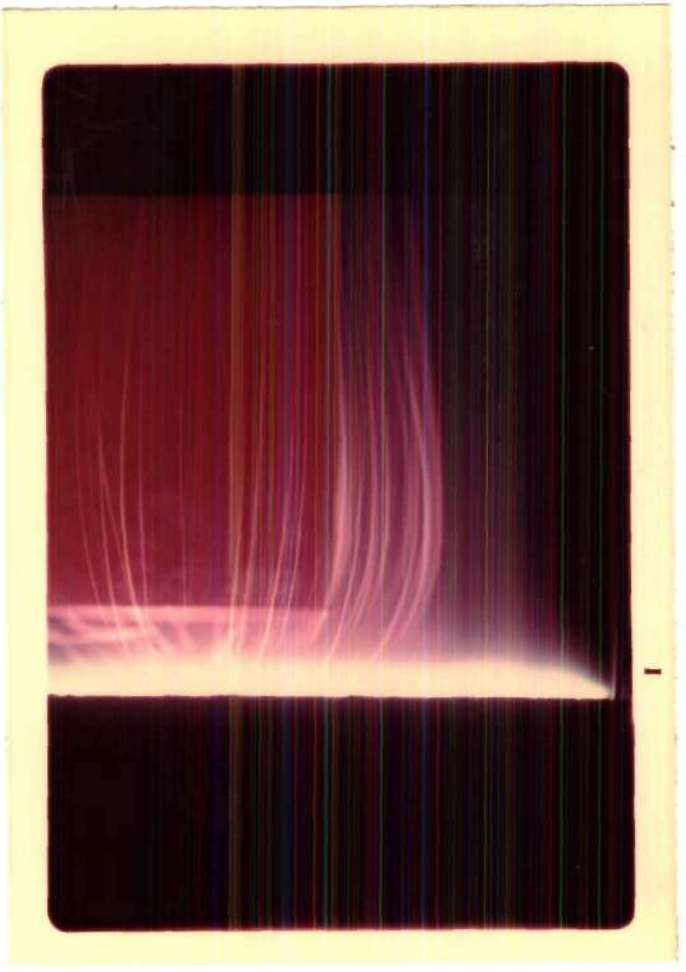

Figure 12. Particle Traces in a Flame with Φ = .720 (Kodak High Speed Extrachrome, Tungsten, EHB 135, ASA 320 with ESP-1 Developing, f 8.0, Exposure 30 sec)

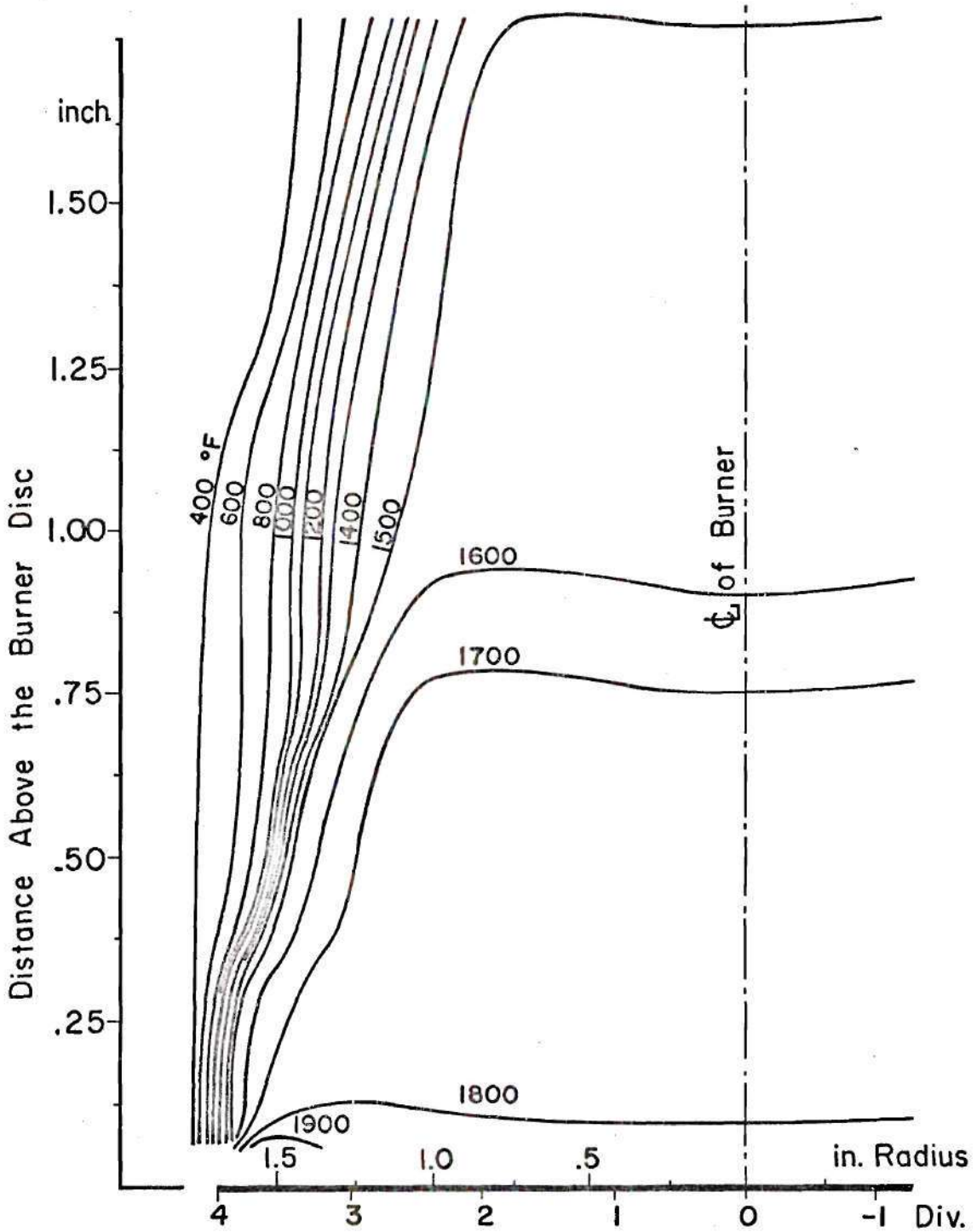

Figure 13. Isothermal Profiles for an Undisturbed Flat Flame. $\Phi = .788$

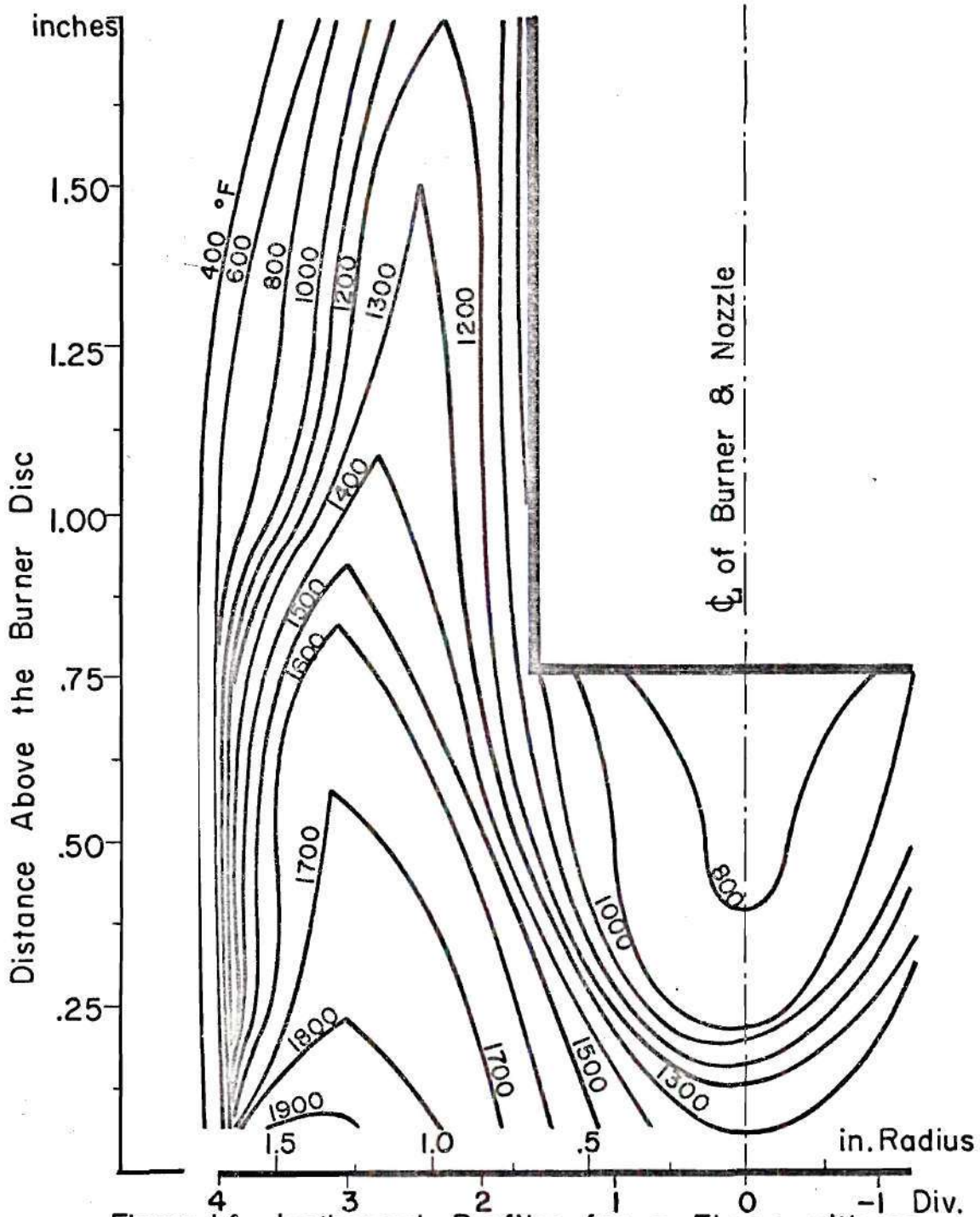

Figure 14. Isothermal Profiles for a Flame with an Opposed N_2 Jet. $\Phi = .788$, $\dot{m}_{N_2} = 607$ Grph.

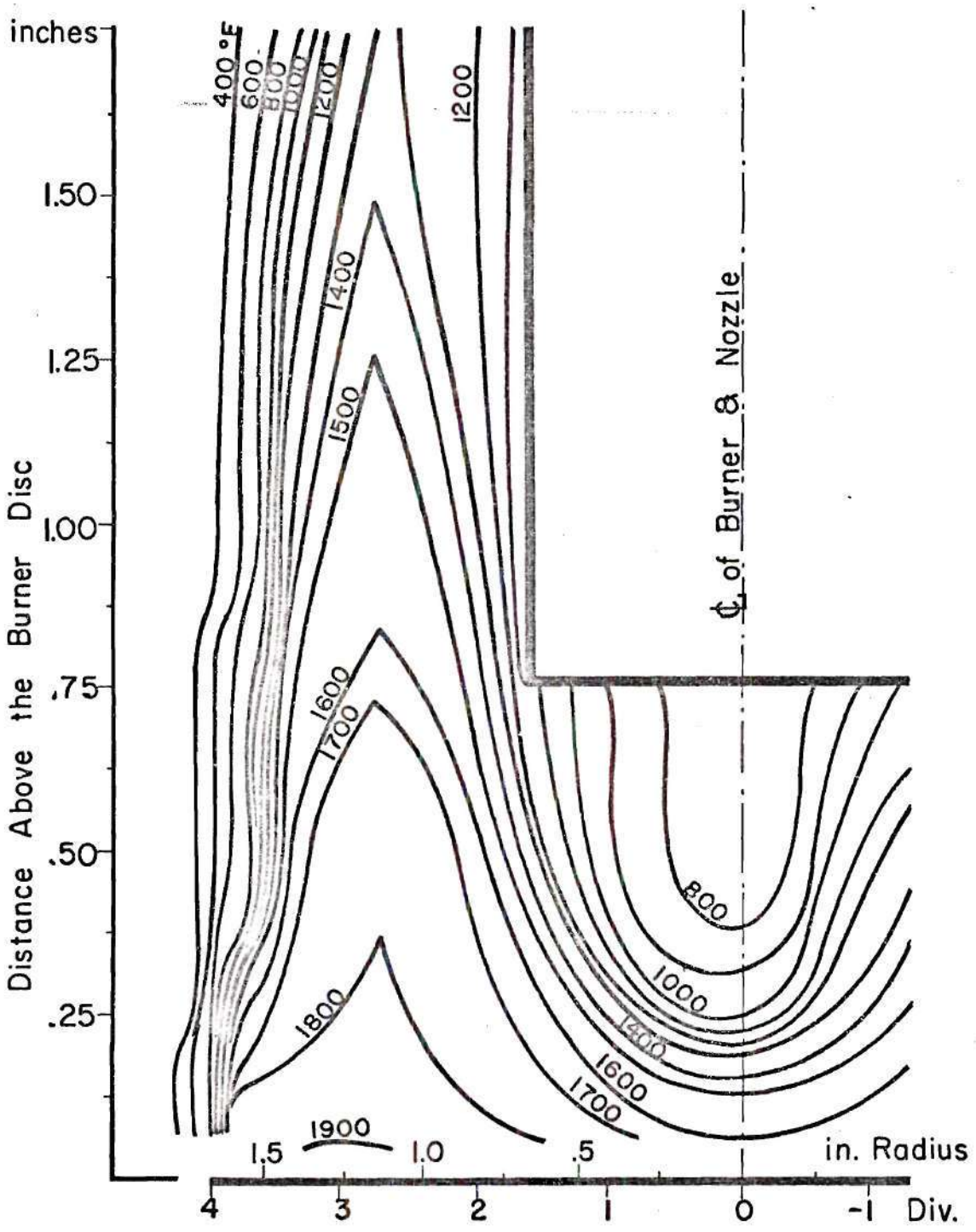

Figure 15. Isothermal Profiles for a Flame with an Opposed N_2—Al Particle Jet. Φ=.788, $\dot{m}_{N2}$=607 Grph , $\dot{m}_{Al}$=3.15 Grph.

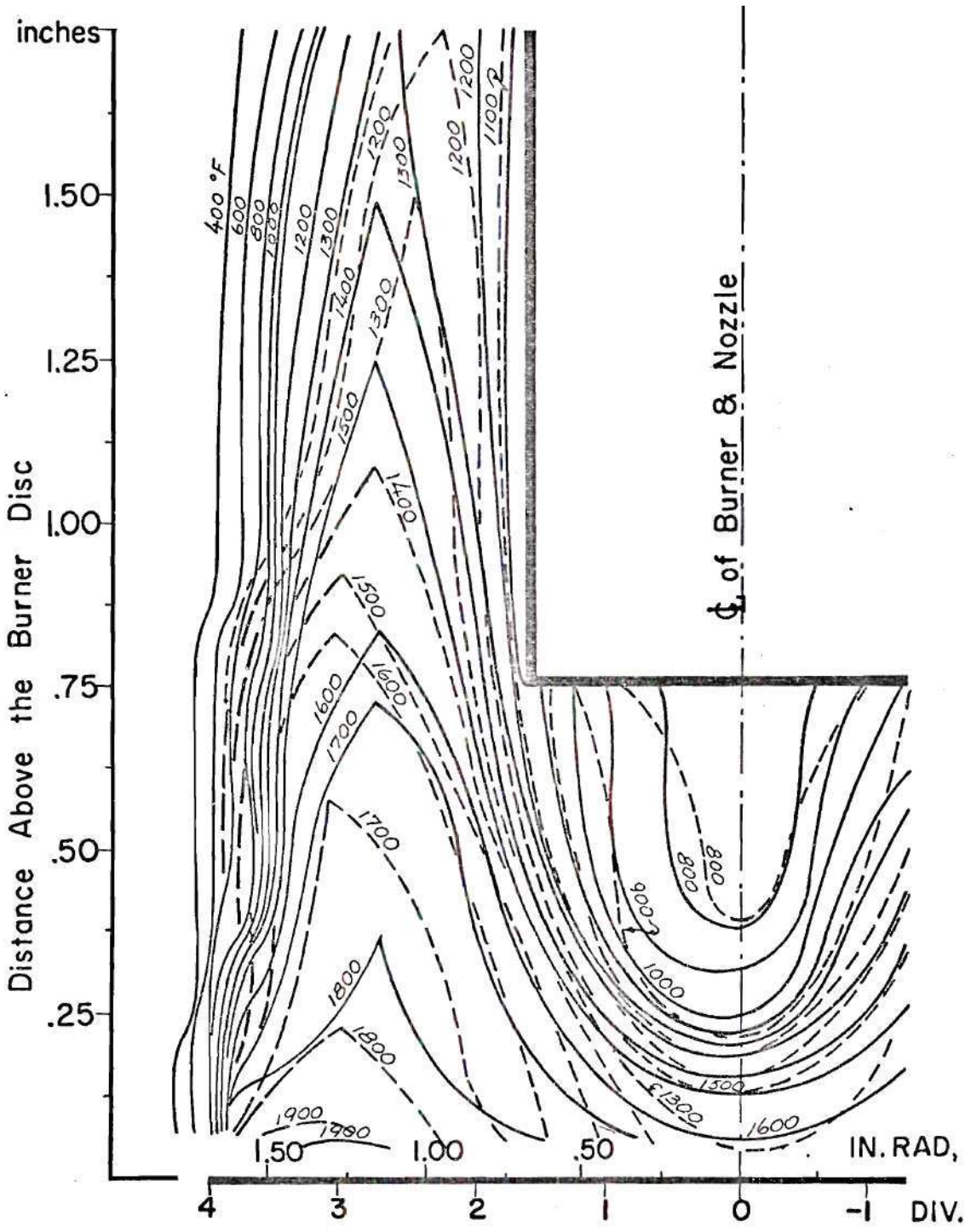

Figure 16. Isothermal Profile Comparison Between a Flame with an Opposed N_2 Jet & one with an Opposed N_2–Al Particle Jet. $\Phi = .788$, $\dot{m}_{N2} = 607$ Grph, $\dot{m}_{Al} = 3.15$ Grph.

B. Estimating Aluminum Particle Reaction

An energy balance was made in an attempt to estimate the percentage of aluminum consumed. Control volumes with an upper boundary at the horizontal planes at $\frac{1}{16}$ and $\frac{1}{8}$ inch high and having the diameter of the burner disc were used. The following assumptions were made:

a) Complete combustion of the methane, with no dissociation, takes place at one atmosphere total pressure.

b) The reactants, air and methane, enter the control volume from the burner disc at a temperature of 298°K.

c) The products of combustion leave the control volume at the mean temperature corresponding to the $\frac{1}{16}$ and $\frac{1}{8}$ inch planes.

d) The nitrogen and the nitrogen-aluminum particle jets enter at the mean temperature corresponding to the center of the $\frac{1}{4}$ inch plane.

e) The oxidizer available to the aluminum particles corresponds to the free oxygen from the methane-air reaction.

f) All radiation losses are to be calculated from the data, and conduction losses are assumed to be of the same order of magnitude as the radiation losses.

The net heats of reaction were calculated first for each flame with the opposed nitrogen jet and then for the flames with the same opposed nitrogen flow and with metal particles added.

The initial step of the calculations assumes that the aluminum particles undergo a heating process without any chemical reaction. The heat of reaction calculated for this reaction was compared with the heat calculated for the flame with only the same opposed nitrogen jet. The difference between the two heats of reaction calculated correspond to

that heat released by the chemical reaction of aluminum to form aluminum oxide. The amount of aluminum that will react depends on the free oxygen available from the methane-air reaction. The amount of aluminum that was consumed was calculated.

If we were to assume that through this reaction, on the average, a pure aluminum core is left, even though an aluminum oxide shell will surround the metal particle, the amount of aluminum consumed will permit calculating the average diameter reduction of the particles.

Table 2 is a summary of the percentage of aluminum consumed and average particle diameter reduction calculated for flames with combustion completion ratios between .914 and .720. It is observed that the aluminum consumed varied between 27.9 and 53.7 percent and the diameter reduction varied between 5.2 and 11.3 micrometers.

C. Photographic Records

The calculated particle mean speeds varied between 5 and 55 inches per second. Near the burner disc their speed is low, in as much as they are injected counter to the flow of the combustion products, they must go through a reversal in their direction. As the particles are consumed they achieve the speed of the reacting gases and they accelerate as they move away from the burner disc.

The mean speed for all metal particles measured was found to be the same for any fixed point above the burner disc and for flames having the same combined mass flow of fuel and air.

Figures 17, 18, and 19 display the calculated particle mean speeds according to their position with respect to the top of the burner disc. Other graphs are presented in the Appendix.

Table 2. Estimating Aluminum Particle Reaction

Φ	v_f	Mass Flow Al	Mass Flow N_2	H	Temperature Edge	Temperature Center	Percentage Aluminum Consumed	Particle Diameter Reduction	Particle Diameter
	cm/s	g/h	g/h	in	°K	°K	%	μm	μm
.914	5.56	9.83	475.8	$\frac{1}{8}$	1231	1012	53.7	11.3	38.7
.788	9.74	8.41	186.8	$\frac{1}{16}$	1348	1208	27.9	5.2	44.8
				$\frac{1}{8}$	1323	1208	29.0	5.4	44.6
.720	6.78	10.29	475.8	$\frac{1}{16}$	1113	981	37.7	7.3	42.7
				$\frac{1}{8}$	1105	981	39.4	7.7	42.3
.720	6.78	7.98	475.8	$\frac{1}{16}$	1133	1014	51.4	10.7	39.3
				$\frac{1}{8}$	1112	1014	41.8	8.2	41.8

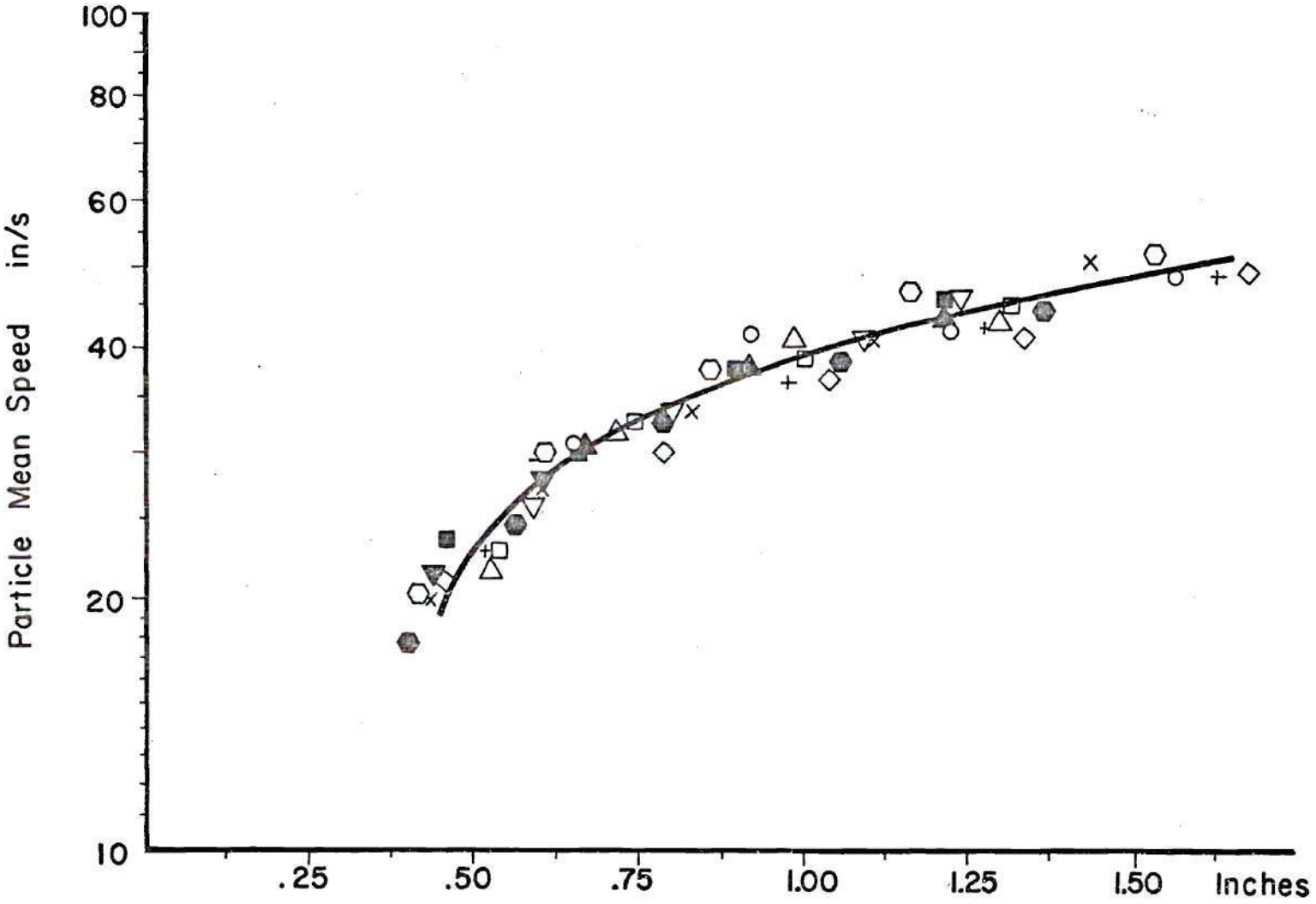

Figure 17. Aluminum Particle Speeds. Φ=.848, V=.218 Fps.

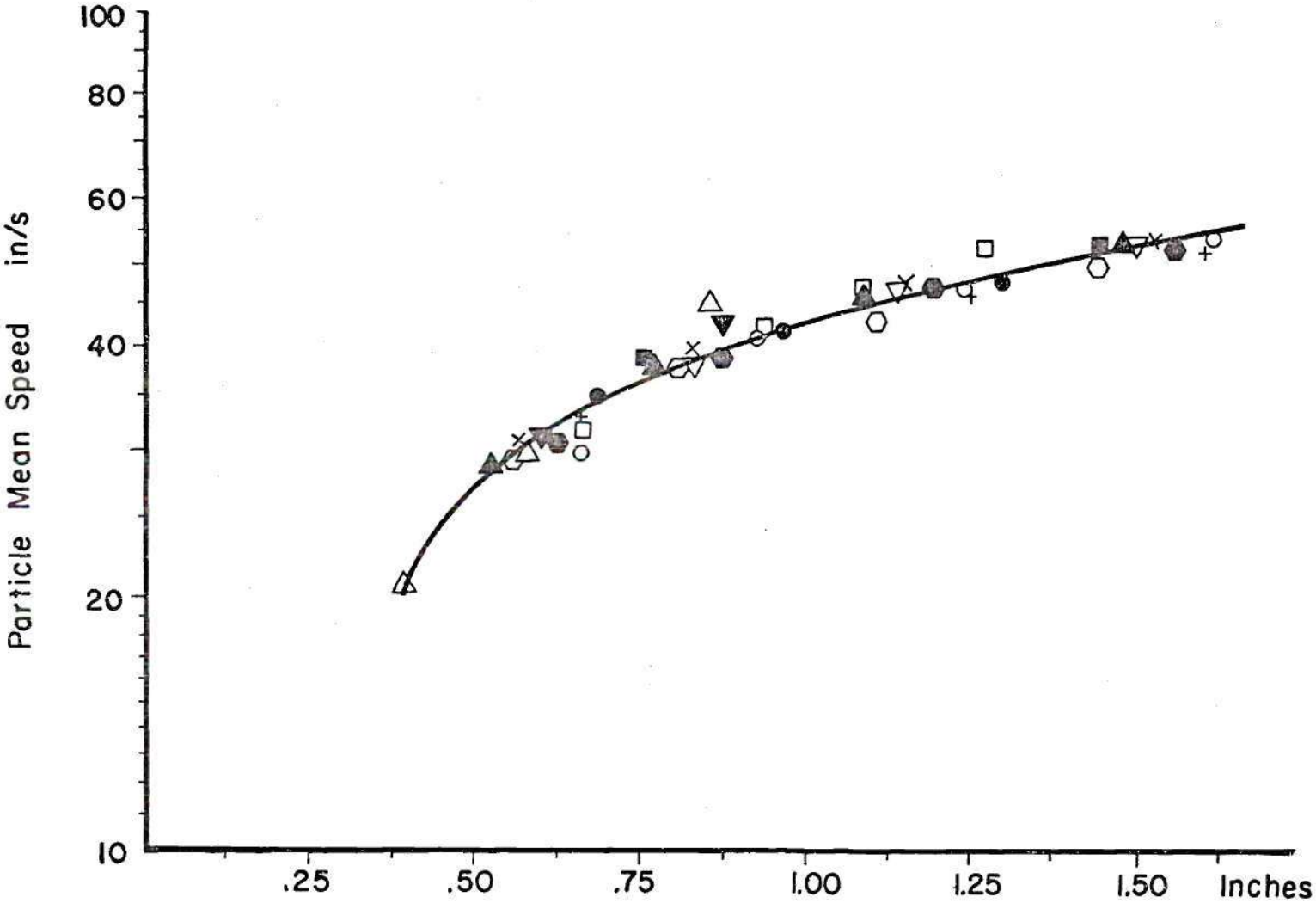

Figure 18. Aluminum Particle Speeds. Φ=.788 , V=.224 Fps.

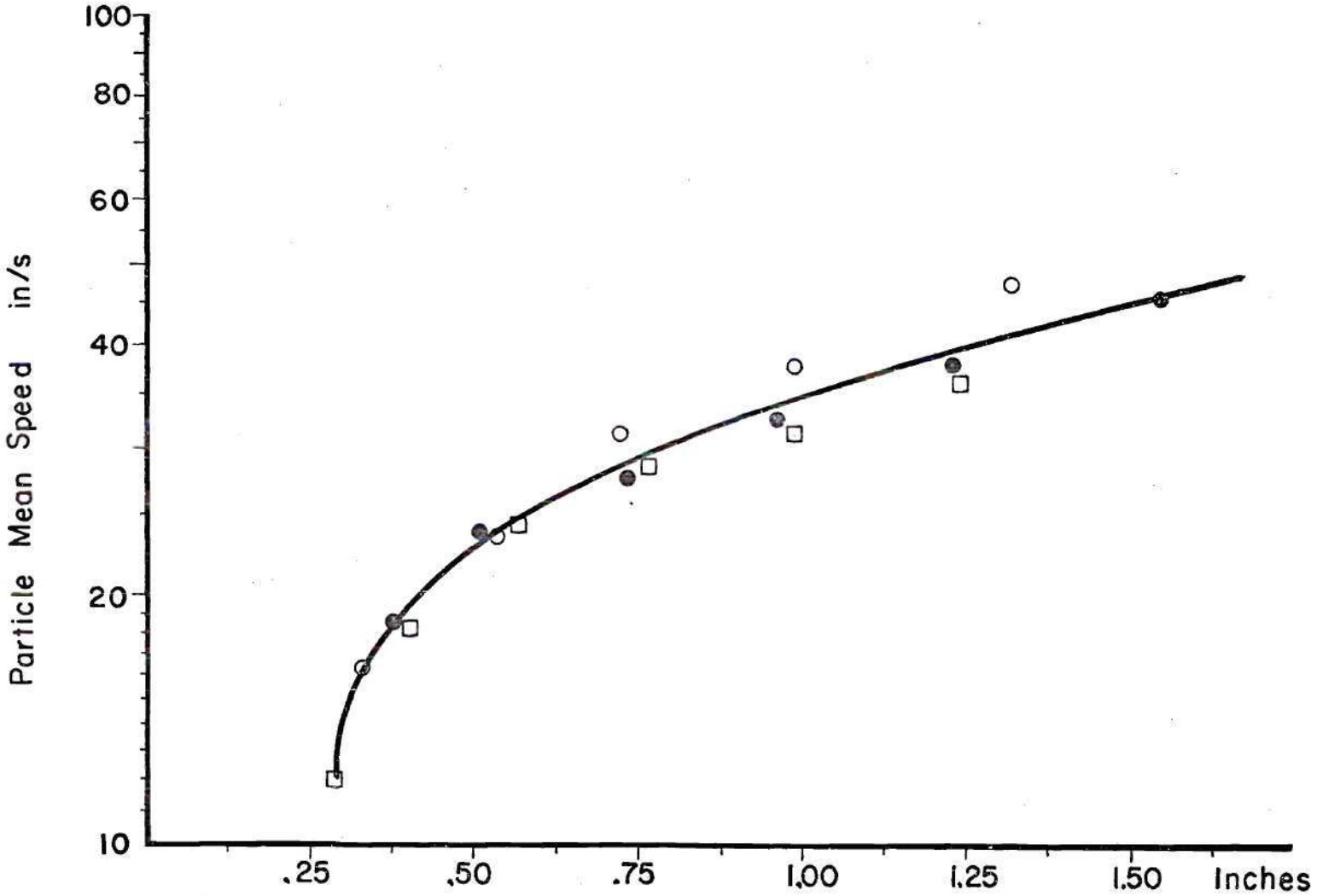

Figure 19. Aluminum Particle Speeds. Φ=.608, V=.210 Fps.

If the curves are extrapolated all the way to the horizontal axis, the point where the particles reverse their direction (zero particle velocity point) can be located. This appears to be between 0.25 and 0.40 inch above the burner disc.

Figure 20 displays four curves showing aluminum particle mean speeds for different combustion completion ratios, nitrogen flow being the same for all four cases. It is apparent from this figure that no trend can be seen of the effect of the air-fuel ratio on the particle mean speed. The calculated gas velocity, on the other hand, orders these curves in the expected direction.

At the lower positions above the burner disc the lines cross. However, no definite conclusions can be reached for this region due to lack of sufficient data. It can be noted from this figure that metal particles reacting in high speed flames have a higher mean speed for any fixed point above the burner disc. The highest speeds were found in a flame with Φ = .788 and a gas velocity of 9.74 cm/sec, while the lowest mean particle speeds were found in a flame with Φ = .720 and a gas velocity of 6.78 cm/sec. It is apparent from these curves that the particles achieve the gas velocity at a point 0.75 inch above the burner disc.

From personal observations and from the photographic records, ignition of particles was observed in flames with mean temperatures as low as 975°K. Ignition was evidenced by the sharp luminosity of their tracks. Figures 11 and 12 display some of this evidence; additional photographic records have been included in the Appendix.

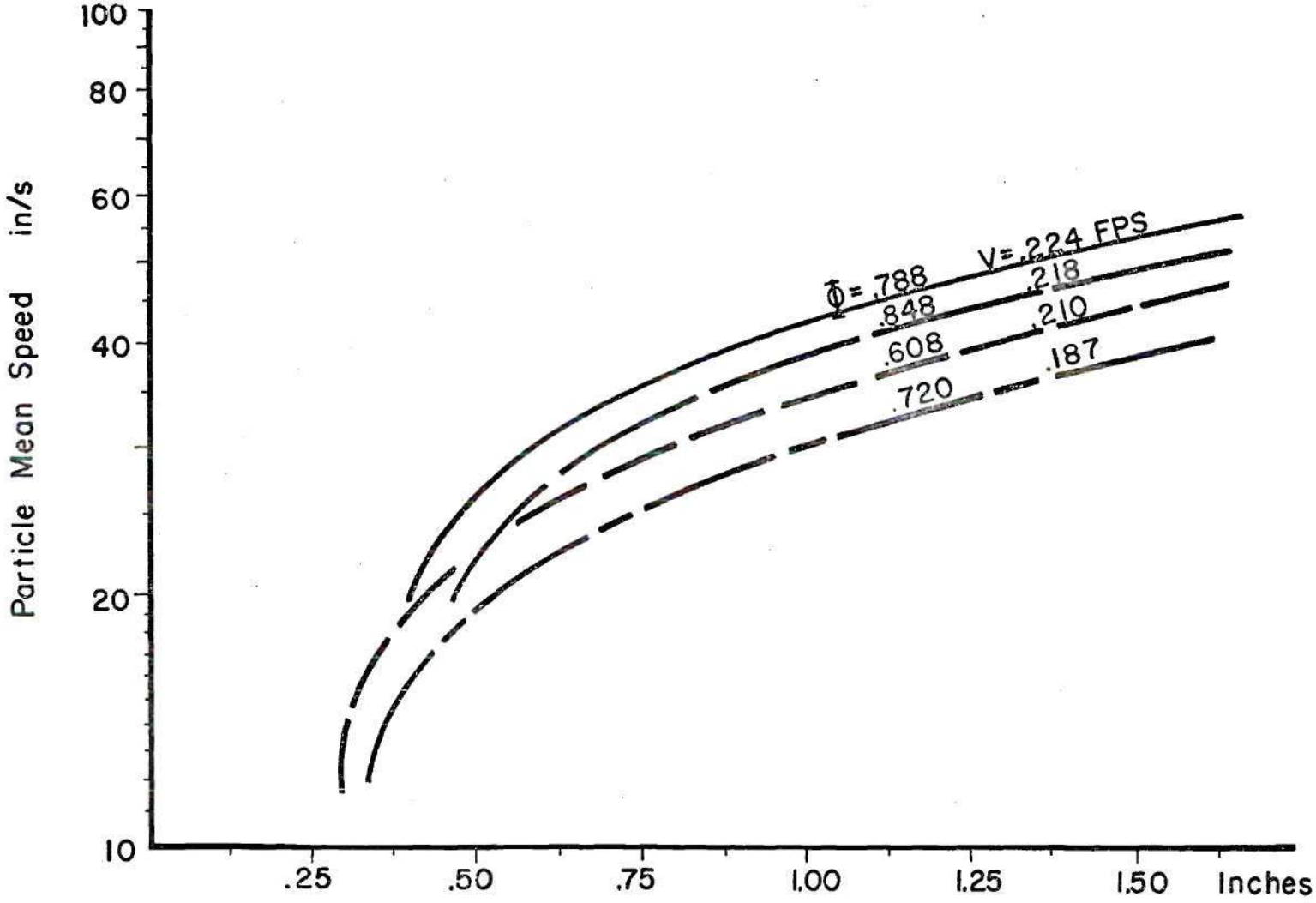

Figure 20. Aluminum Particle Speeds, Comparison for Different Combustion Completion Ratios.

In reviewing the literature, aluminum particle macroscopic movements such as spinning and fragmentation were reported (3). These were attributed to rapid heating of the metal particles that caused the oxide layer to crack and burst accompanied with changes in the particles' path. In the present work, these phenomena were not observed nor captured on the photographic records.

D. Effect of Cooling Nitrogen Flow

In the initial planning of this experimental program it was considered desirable to introduce some control in the gases between the burner tube and the pyrex glass chimney. It was for this reason that, as discussed in the second chapter, nitrogen was introduced through the modified supporting table.

Tests were conducted making temperature measurements for the three phases of this experimental investigation. In all these runs it was found that the external flow of nitrogen distorted the temperature field and disturbed the path of the reacting aluminum particles. Figure 21 shows the isotherms for a flame with an opposed nitrogen jet and a combustion completion ratio of .788. Nitrogen was introduced through the supporting table.

If one compares Figure 21 with Figure 14, which displays the isothermal curves for a flame with an opposed nitrogen jet and with no nitrogen circulation between the burner tube and the glass chimney, the irregular isotherms are very much in evidence in the former. The disturbed particle paths were detected from personal observations. It was for this reason that the external cooling nitrogen flow was eliminated

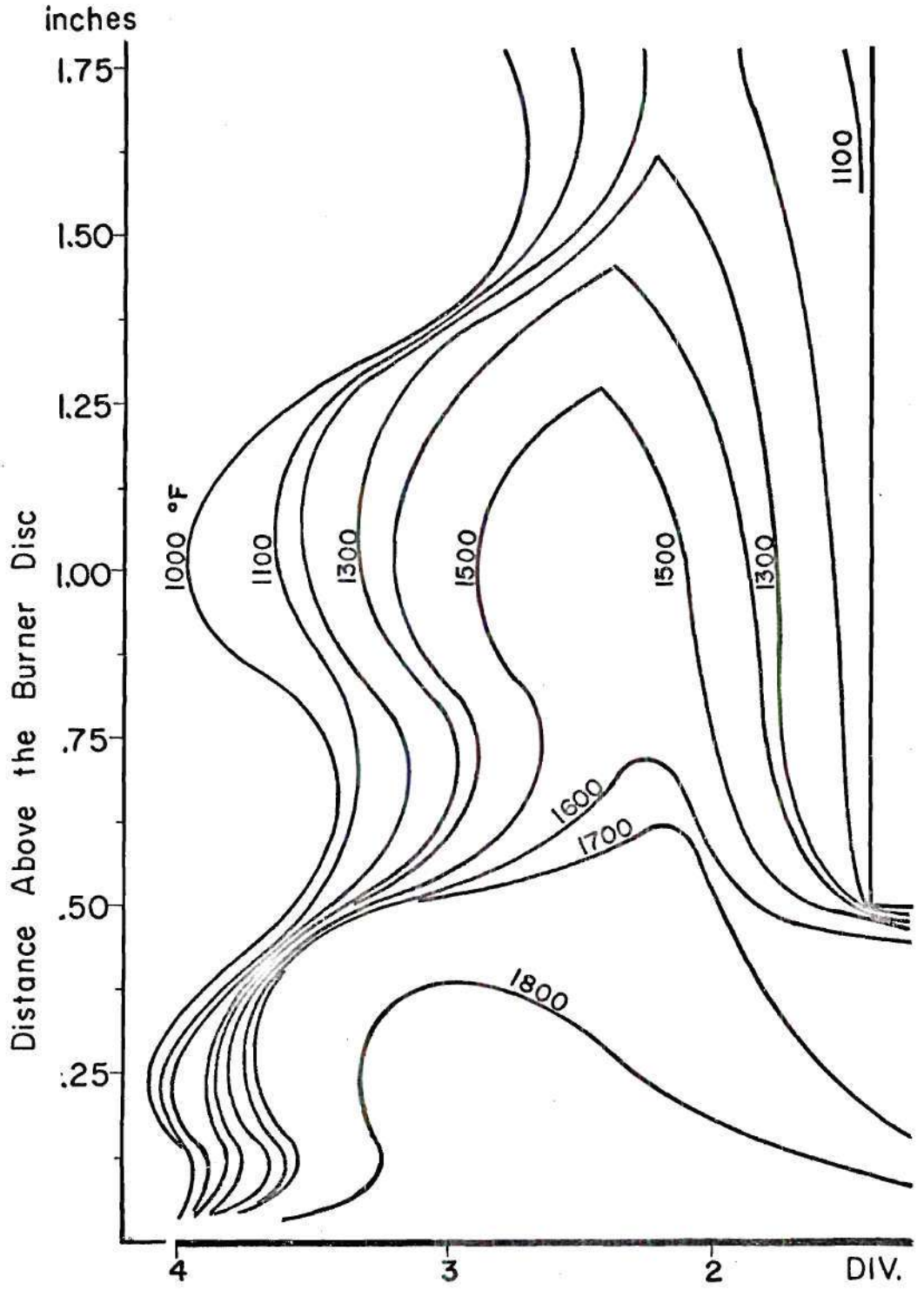

Figure 21. Isothermal Profiles for a Flame with an Opposed N_2 Jet & Cooling N_2 Circulating Between Burner Tube & Chimney.

and air was allowed to flow freely between the burner tube and the chimney.

E. Temperature Profile of an Undisturbed Flame with a Plugged Burner Disc

After some period of experimentation with particle injection, it was observed that the burner porous bronze disc would tend to plug up due to particle accumulation. In order to prevent continuation of experiments with a plugged disc, temperature measurements were periodically made at the reaction zone for an undisturbed flame. The profiles obtained were compared with previous profiles for the same disc. Figure 22 compares two such profiles. It is apparent that the flat profile represents one obtained with an unplugged disc while the other corresponds to one obtained using a severely plugged disc.

It should be noted that the burner discs were discarded before they reached this level.

Another point of interest from Figure 22 is that the temperature readings at the edges of the plugged disc were higher due to higher velocities of the air-fuel mixture in this region compared to those existing at the center of the disc.

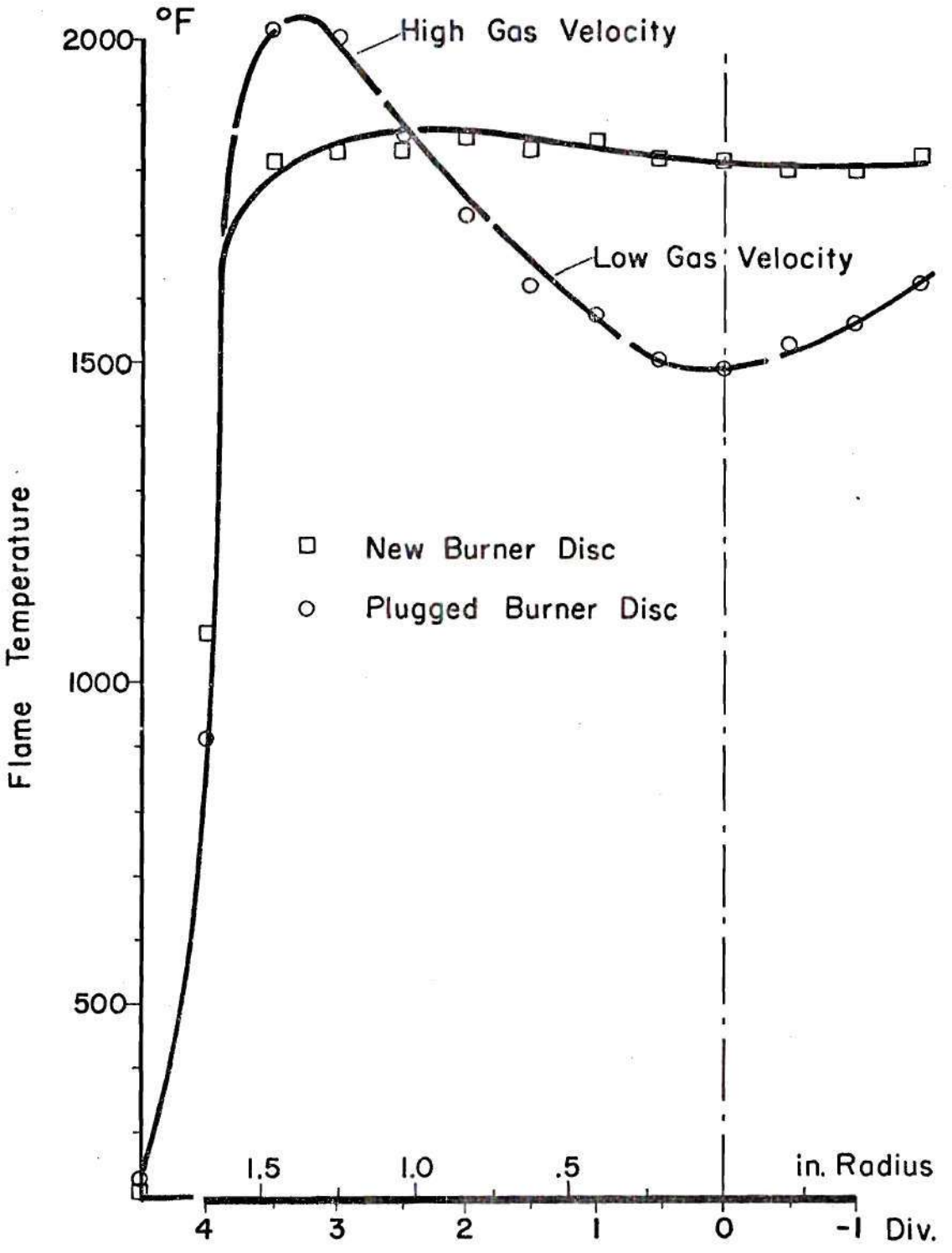

Figure 22. Reaction Zone Temperature Comparison for an Undisturbed Flat Flame Using a New & a Plugged Burner Disc. $\Phi = .788$

CHAPTER V

CONCLUSIONS

The flame and gas temperatures depend both on the flame's combustion completion ratio and on the gas velocity calculated from the combined air-fuel volumetric flow.

A temperature increase was detected for flames having combustion completion ratios between .91 and .72 and with 7 to 12 g/h of aluminum particle flow. This temperature increase results when the energy released from the exothermic reaction of aluminum exceeds the energy absorbed by the combined nitrogen-metal particle flow.

A temperature decrease was detected for flames having combustion completion ratios of .608 and lower and with the same mass flows of metal particles. This temperature decrease results when the energy released from the reaction of aluminum does not exceed the energy absorbed by the combined nitrogen-aluminum particle flow.

Flames with a mean temperature of about 980°K or higher were found to result in an excess of energy release from the exothermic reaction of the aluminum particles.

Particle ignition was evidenced by the sharp luminosity of the metal particle tracks. It was observed that the ignited particles were more numerous in the rich side of the combustion completion ratio compared to the lean region.

The larger portion of aluminum consumption occurs directly under

the particle injection nozzle. The energy balance performed in the reaction zone permitted the estimation of aluminum consumption in this region; the estimated percentage of aluminum consumed varied between 27.9 and 53.7 for this experimental investigation.

The measured particle mean speeds varied between 5 and 60 in/s and were higher in flames having higher gas velocity. The effect of the air-fuel ratio on the particle mean speeds is not apparent due to the fact that many other variables changed at the same time in the tests that were conducted. Particles accelerate as they depart from the burner disc and they appear to achieve the gas velocity shortly after they reverse their paths.

The portion of zero particle speed can be obtained by extrapolating the particle speed plots. This position was found to range between 0.25 and 0.40 inch above the burner disc for the experiments conducted in this work.

Plugged discs can be detected by comparison of successive profiles of the undisturbed flame.

Nitrogen flow between the burner tube and the glass chimney will distort the flame's temperature field and disturb the paths of the reacting aluminum particles.

CHAPTER VI

RECOMMENDATIONS

The support for the traversing mechanism must be redesigned with axial and radial adjusting mechanisms.

For temperature measurements in horizontal planes higher than two inches above the burner disc, a port hole six inches high is recommended. The diaphragm must be fixed to the chimney with a screw-nut system since the method used in this work was not satisfactory.

The burner porous disc assembly should be redesigned for a better seal between the disc and the supporting ring. The system used in this work did not provide a good seal, epoxy was used to avoid methane-air leakage between the disc and the ring.

Due to heat conduction through the burner tube, the transition nozzle overheated after long operating periods. A water cooled burner tube or transition piece is recommended.

The powder feeder unit is not appropriate for the type of experiments being performed in this burner; it should be replaced by a unit that will deliver a constant, adjustable, and metered low mass flow of metal particles with a low flow of carrier gas.

Pt-13% Rh thermocouples should be used for more accurate temperature measurements. The thermocouples should be coated with a non-reacting, non-catalytic material which would extend the life of the

thermocouple. Also, the possibility of using a temperature recording mechanism should be studied.

In future tests the air-fuel ratio should be varied in such a way that the total combined volumetric flow of air and methane does not vary; a constant gas velocity should be attained for the flames. Also, the combined flow of metal particles and carrier gas should be constant for better comparison between different flames.

Concentration profiles should be determined to complement the temperature profiles and consequently this could be used to calculate net reaction and heat release rates.

Aluminum, aluminum oxide, magnesium, and magnesium oxide particles of different diameters should be used in future experiments for comparison.

A better understanding of the phenomena involved will permit obtaining higher temperatures from the conventional fuels by the addition of metal particles. Also, it should aid in the prevention of metal dust explosions, as well as in the control and burning of metal particles from industrial exhaust gases.

APPENDIX A

TEMPERATURE PROFILES AND PARTICLE MEAN SPEED CURVES

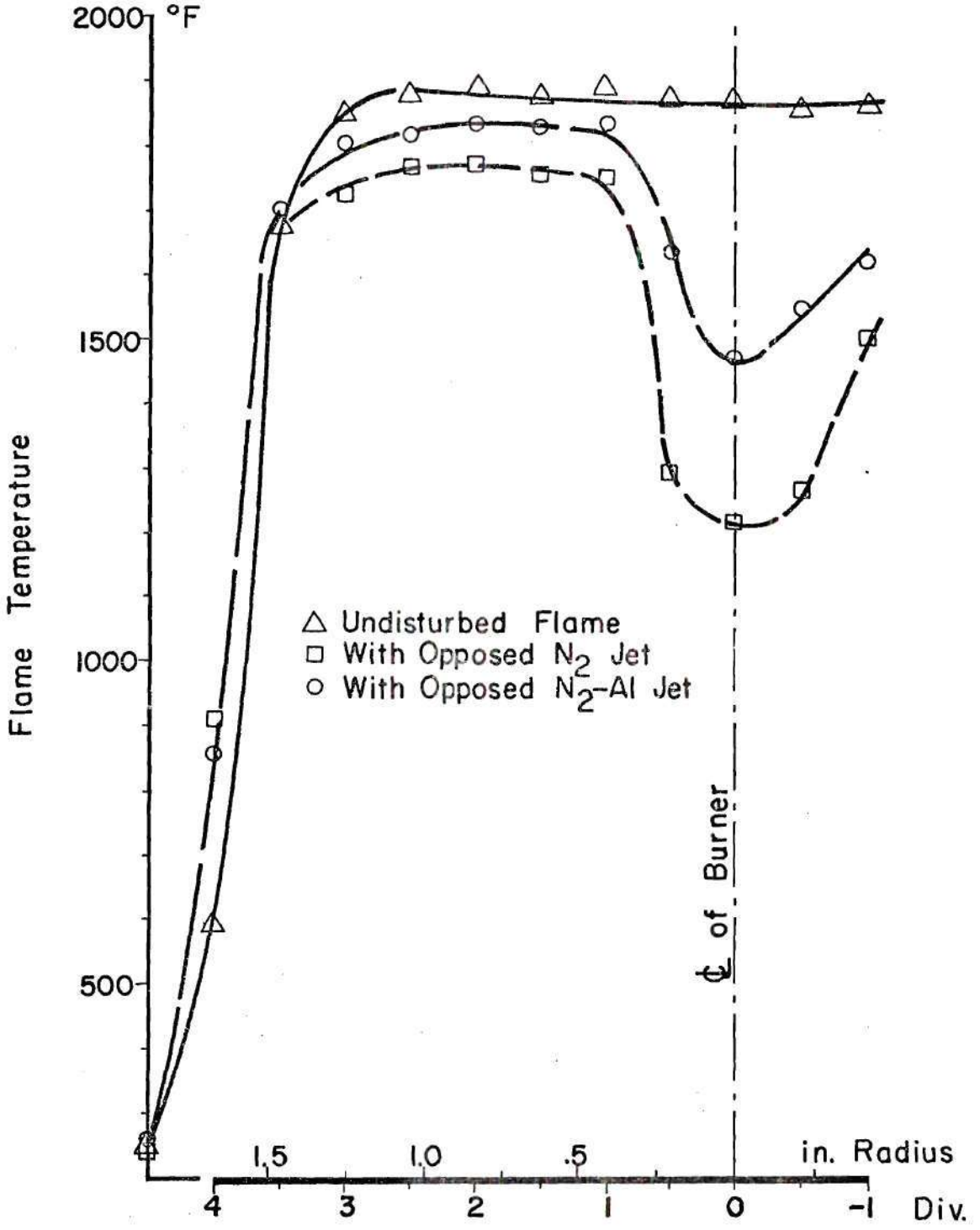

Figure AI. Temperature Profiles. $\Phi = .914$, $\dot{m}_{N2} = 475.8$ Grph
$\dot{m}_{Al} = 9.83$ Grph, V = .164 Fps, H = 1/8 in.

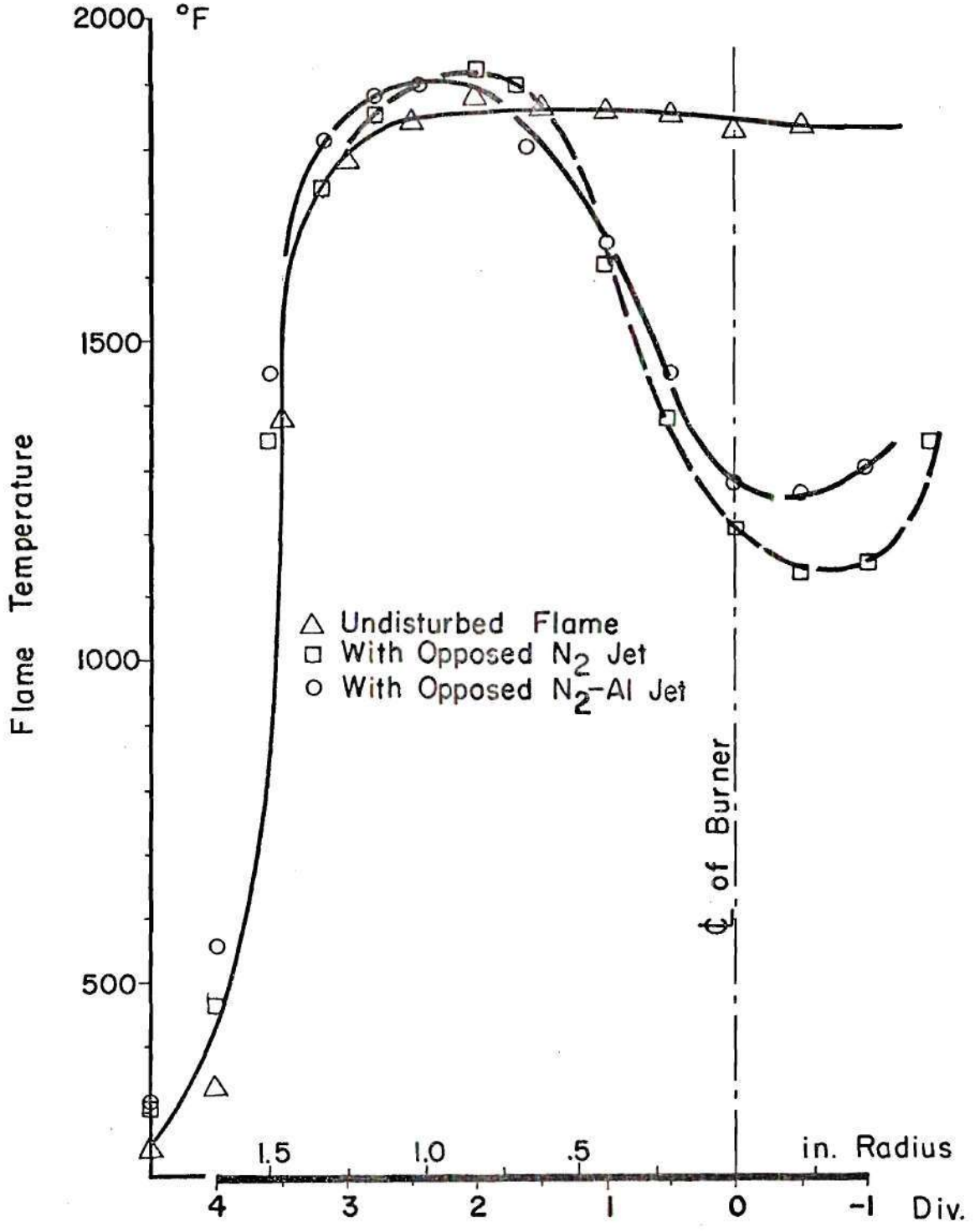

Figure A2. Temperature Profiles. $\Phi = .788, \dot{m}_{N2} = 186.9$ Grph
$\dot{m}_{Al} = 8.41$ Grph, V = .225 Fps, H = 1/2 in.

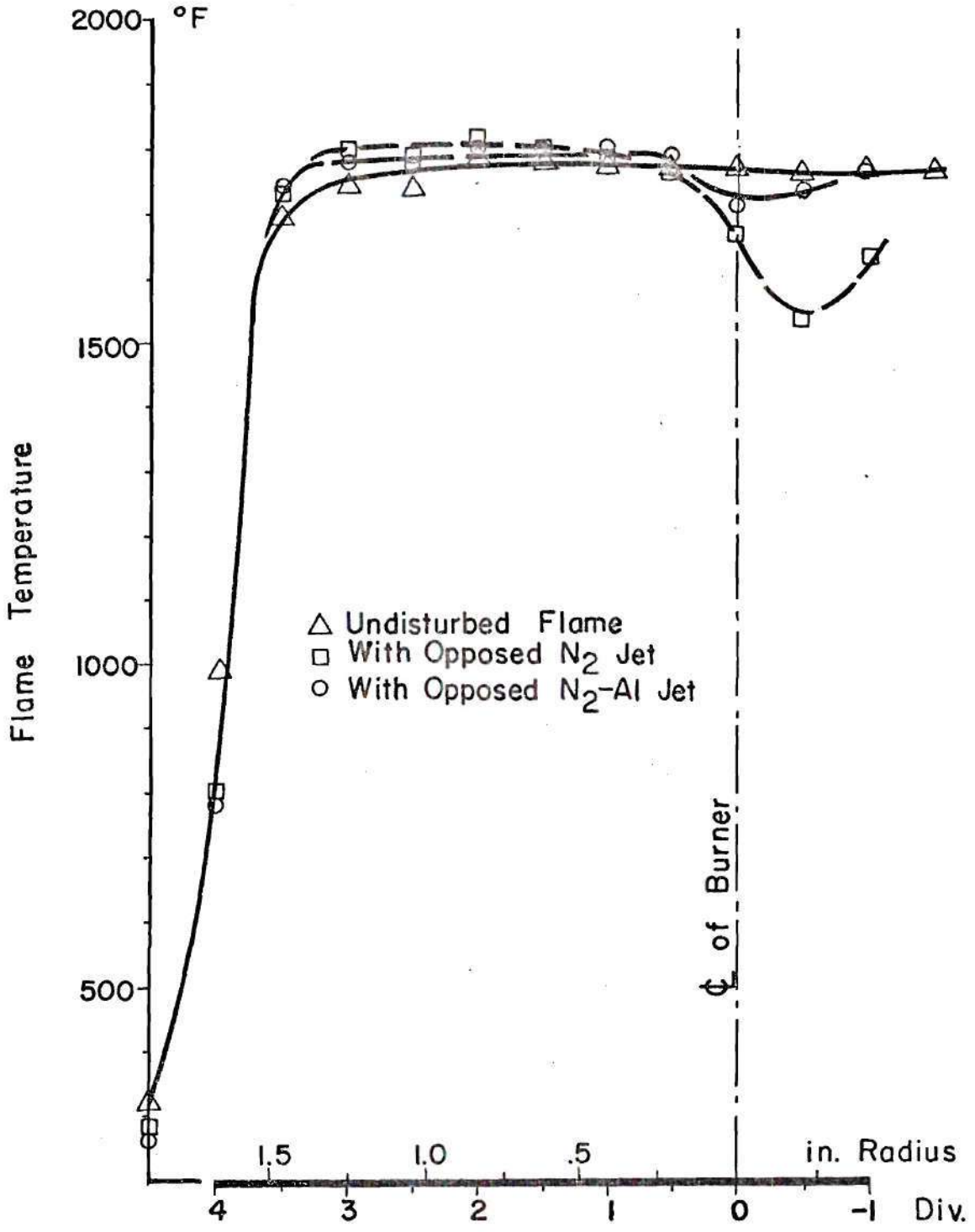

Figure A3. Temperature Profiles. Φ = .720, $\dot{m}_{N2}$ = 136.1 Grph, $\dot{m}_{Al}$ = 12.05 Grph, V = .185 Fps, H = 1/16 in.

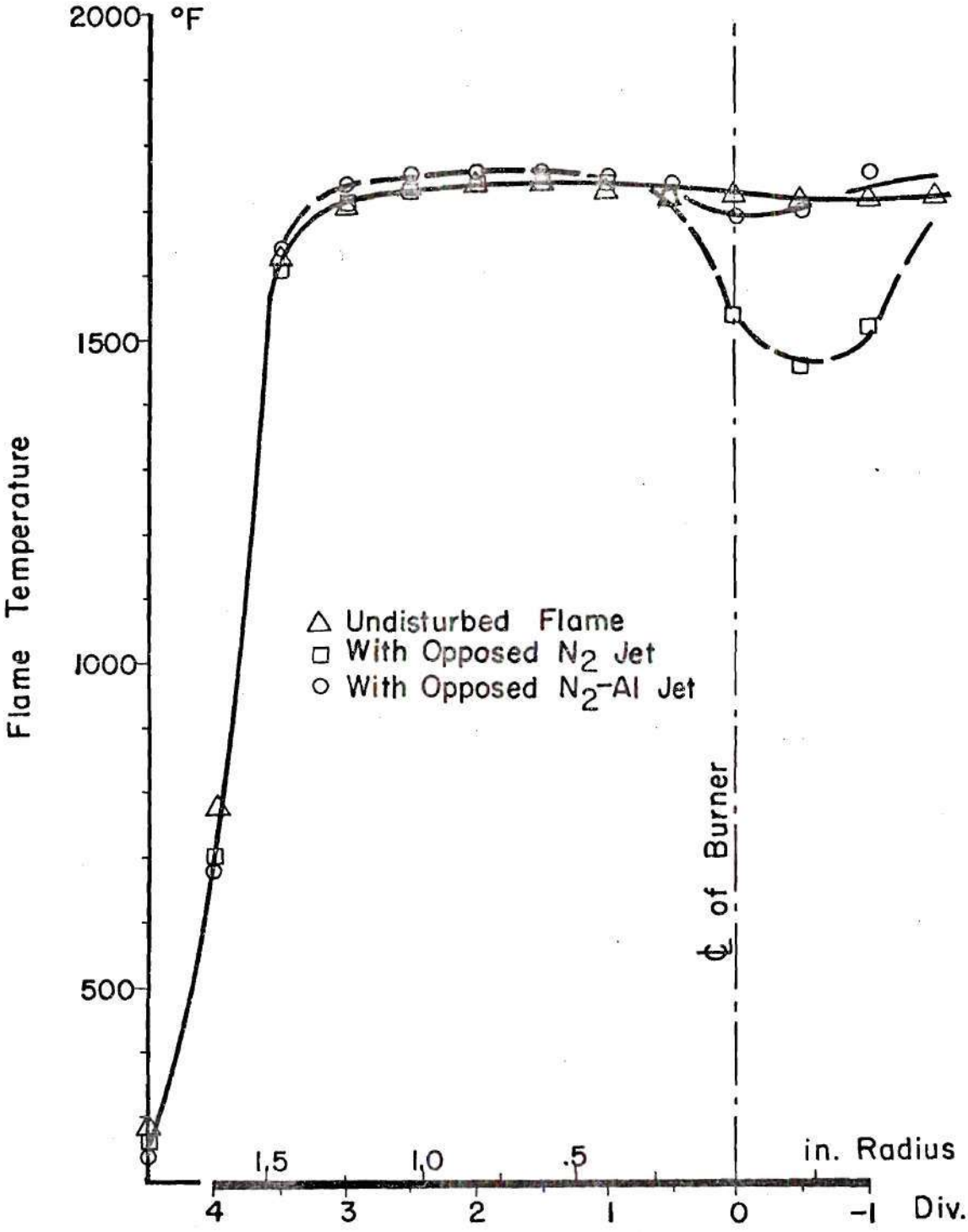

Figure A4. Temperature Profiles. Φ=.720, $\dot{m}_{N2}$= 136.1 Grph, $\dot{m}_{Al}$=12.05 Grph, V=.185 Fps, H=1/8 in.

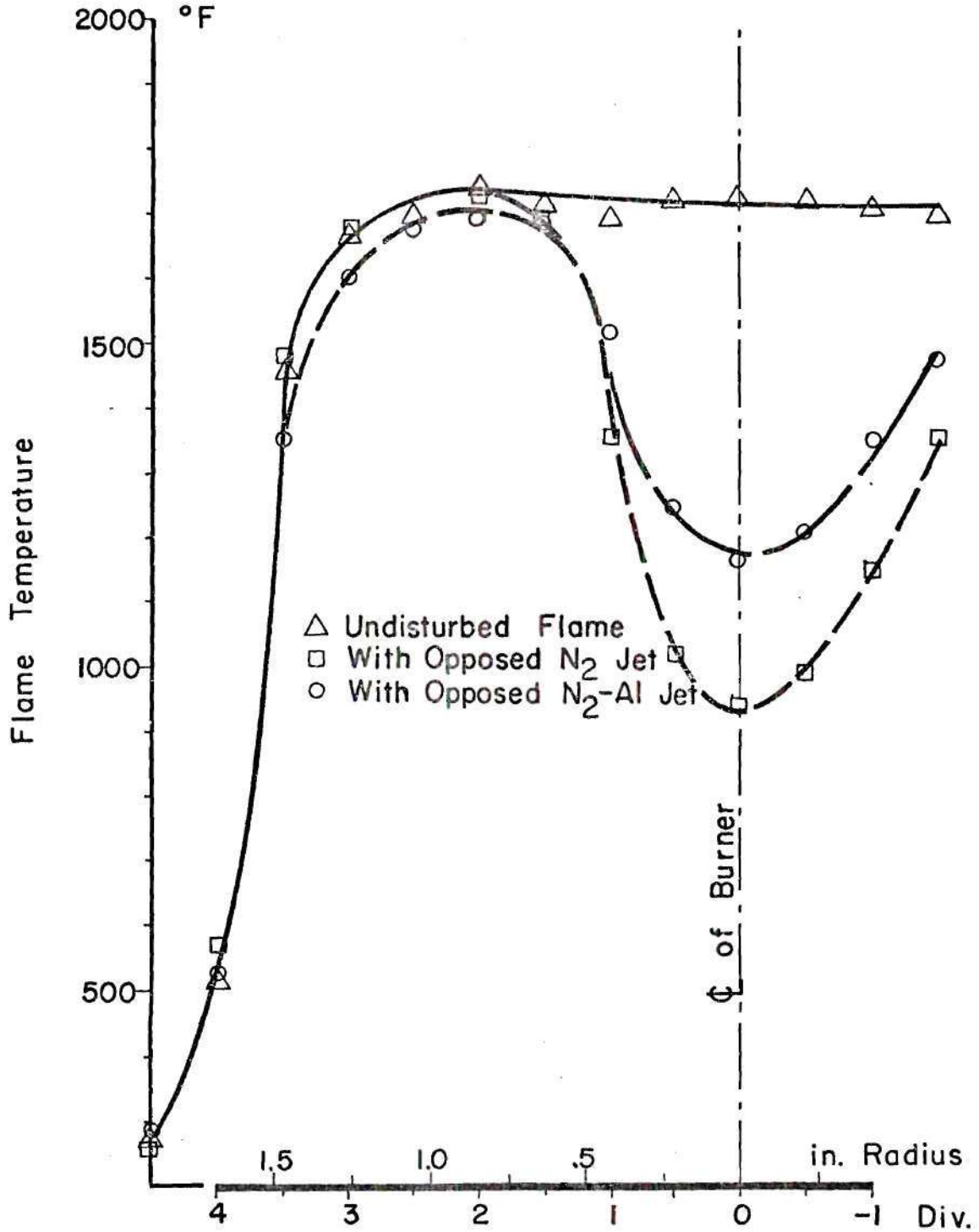

Figure A5. Temperature Profiles. Φ=.720, $\dot{m}_{N2}$=475.6 Grph, $\dot{m}_{Al}$=10.29 Grph, V=.185 Fps, H=1/4 in.

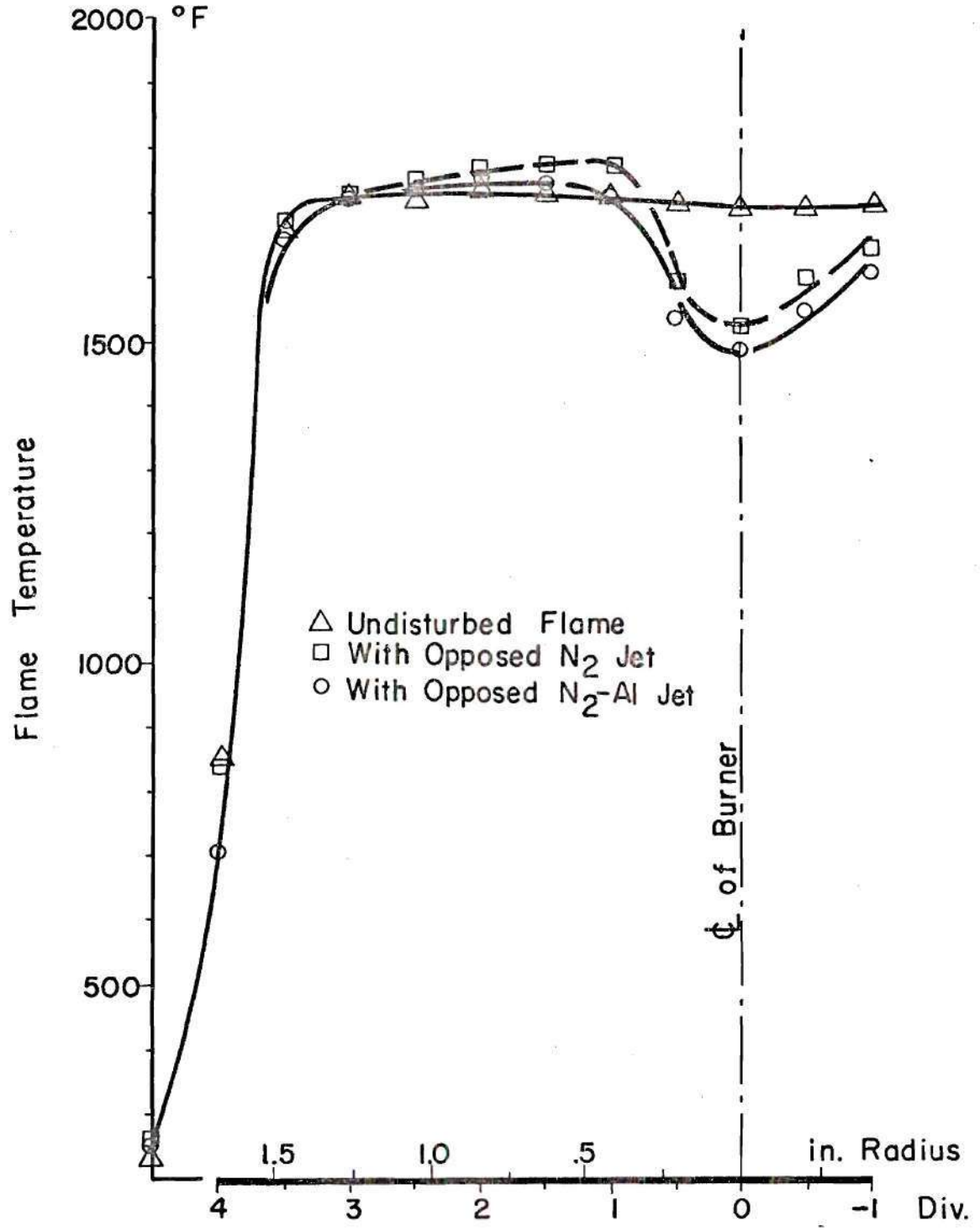

Figure A6. Temperature Profiles. $\Phi = .608, \dot{m}_{N2} = 475.6$ Grph, $\dot{m}_{Al} = 7.82$ Grph, V=.210 Fps, H=1/8 in.

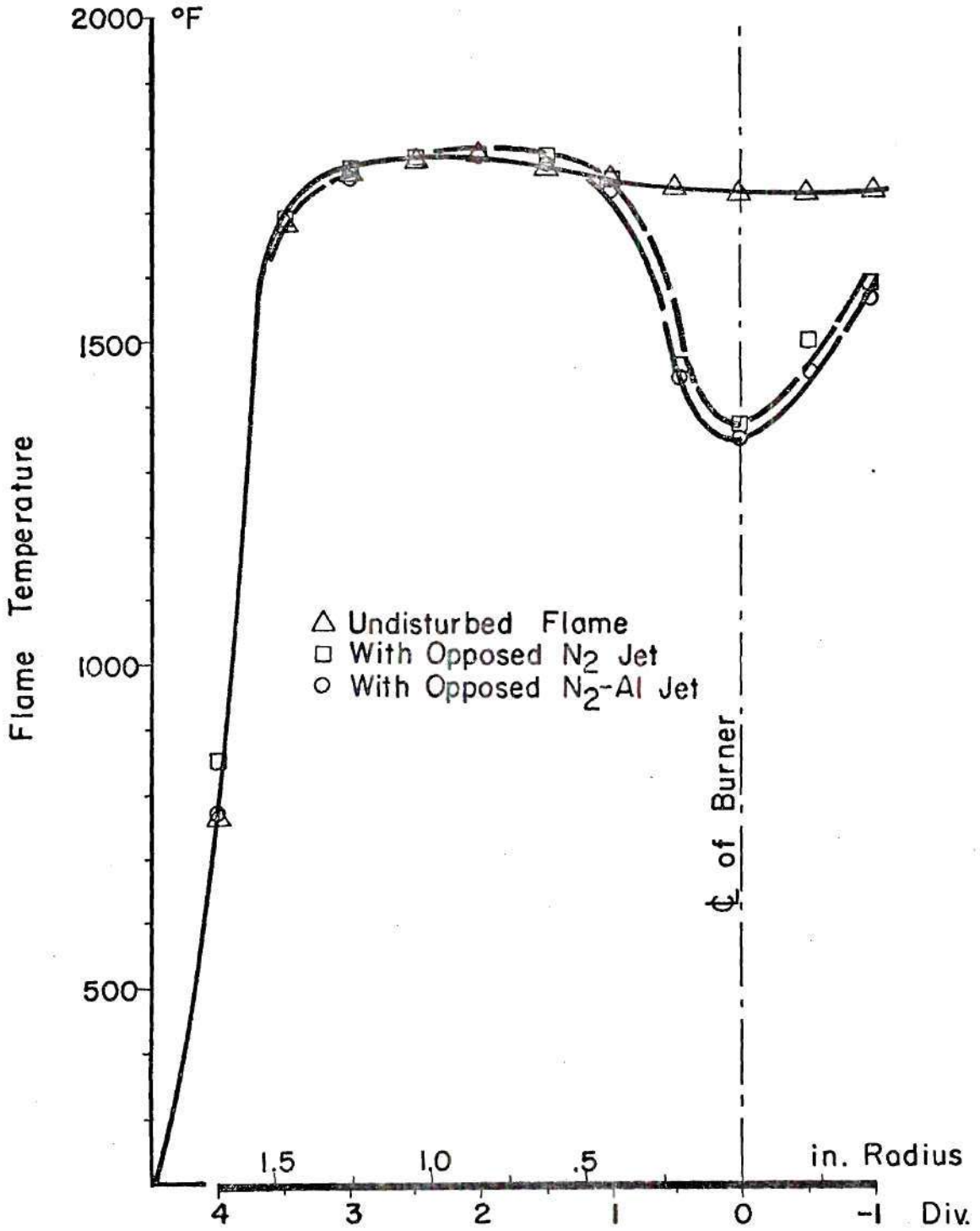

Figure A7. Temperature Profiles. $\Phi = .556, \dot{m}_{N2} = 475.8$ Grph, $\dot{m}_{Al} = 8.56$ Grph, V=.216 Fps, H=1/8 in.

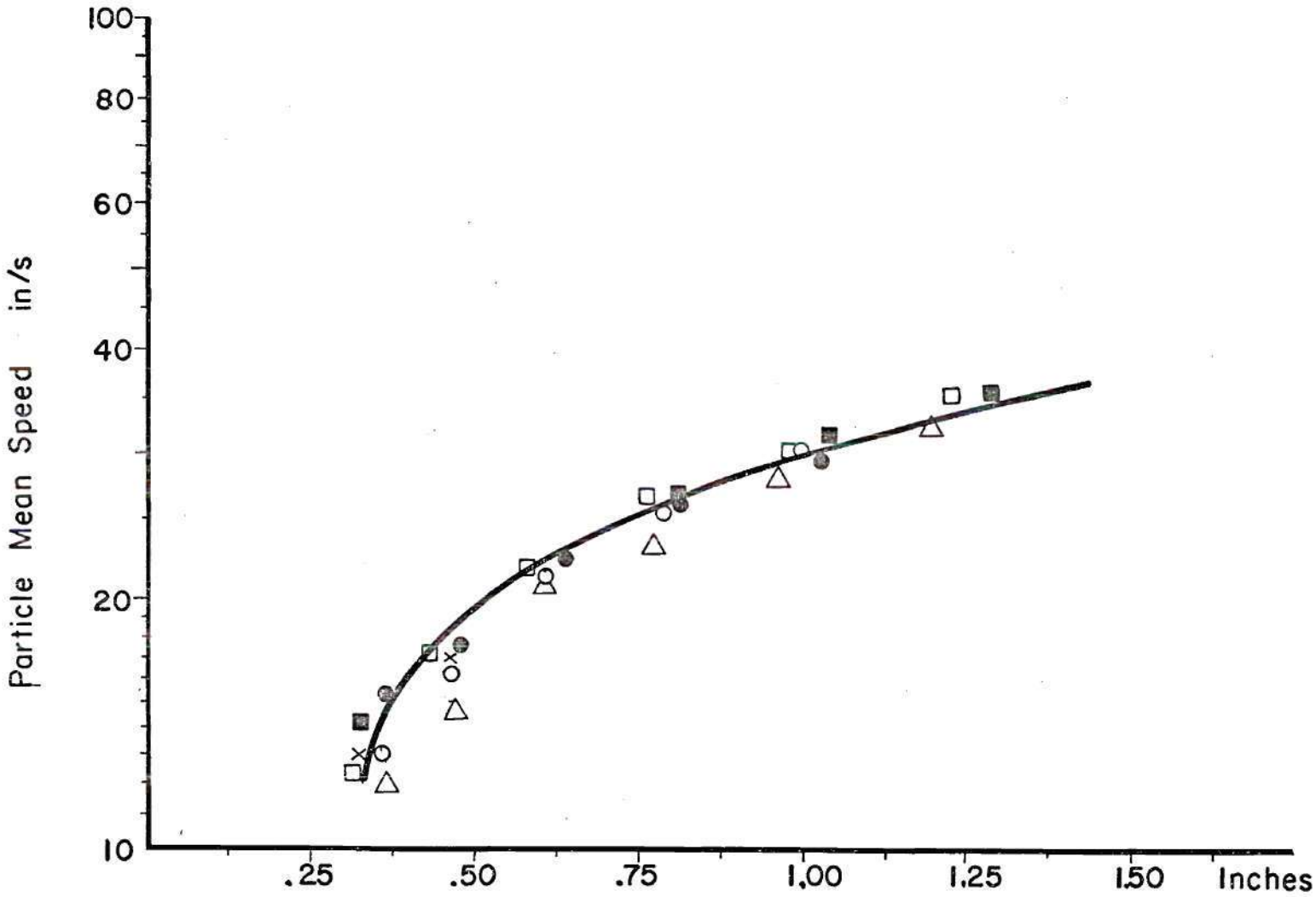

Figure A8. Aluminum Particle Speeds. Φ=.720, V=.187 Fps.

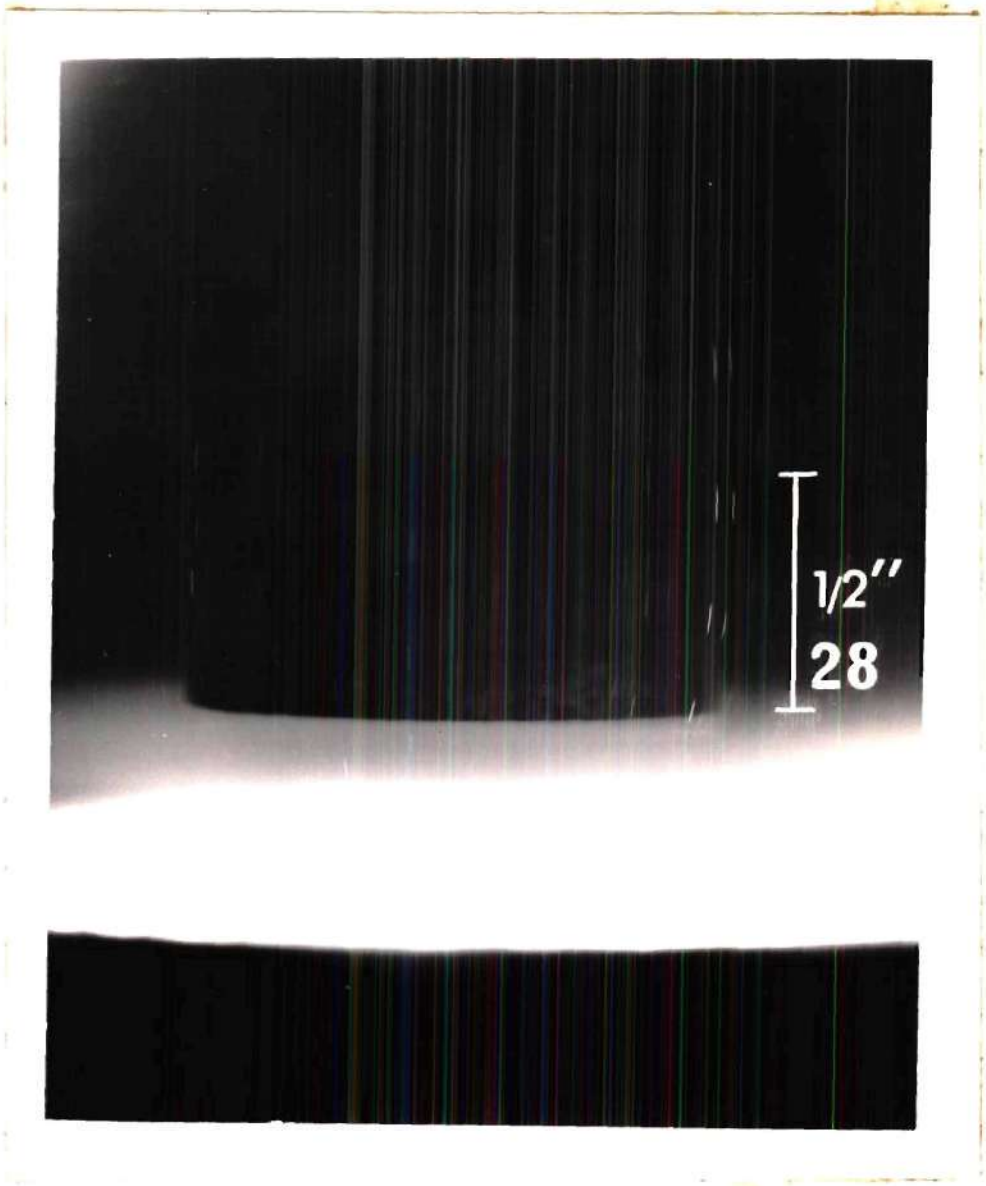

Figure A9. Particle Traces in a Flame with Φ = .848
(Kodak Royal-X Pan, f 4.7, Exposure 10 sec,
Chopper Revolutions 4030)

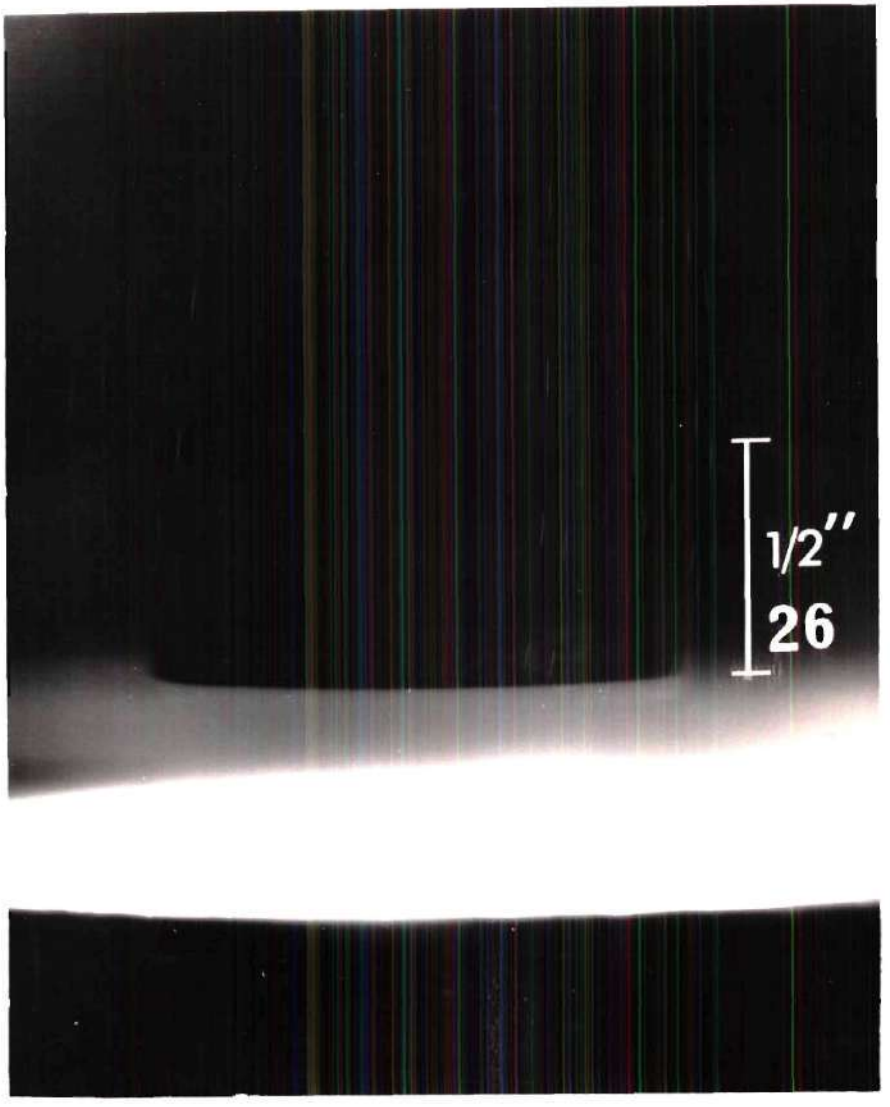

Figure A10. Particle Traces in a Flame with Φ = .788 (Kodak Royal-X Pan, f 4.7, Exposure 10 sec, Chopper Revolutions 4040)

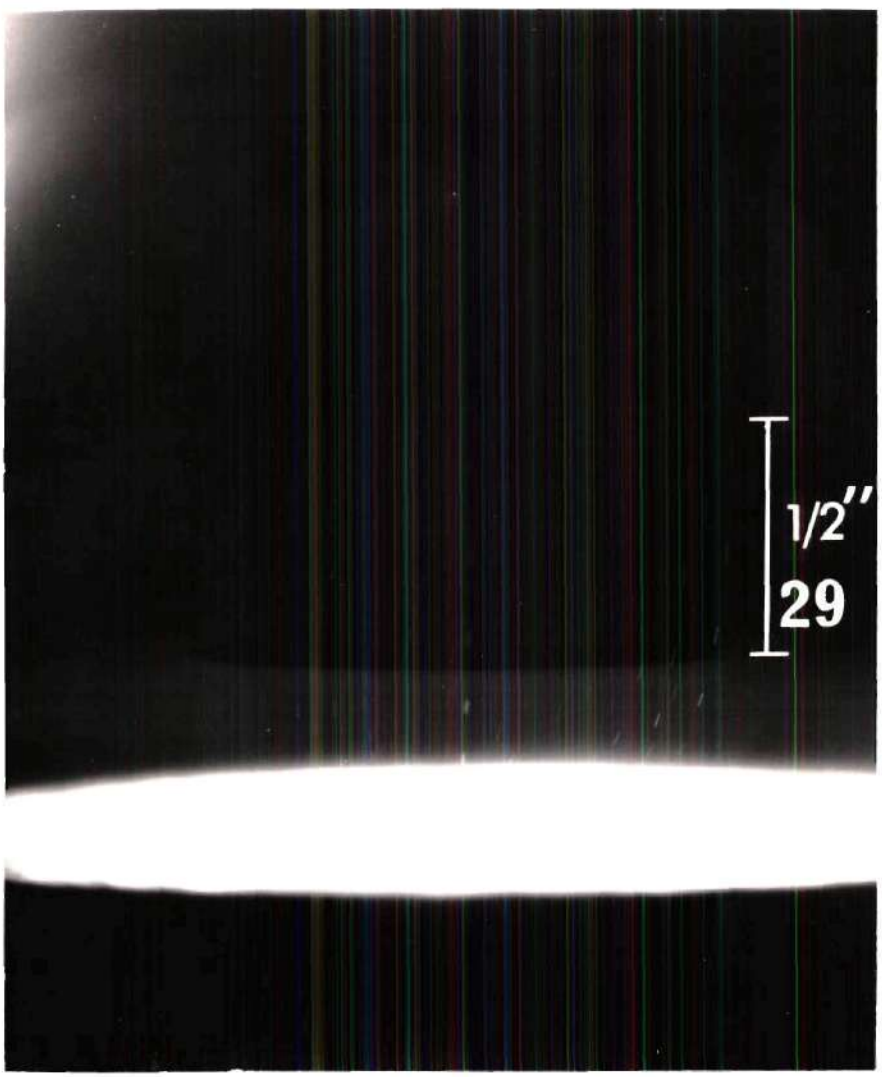

Figure A11. Particle Traces in a Flame with Φ = .720 (Kodak Royal-X Pan, f 4.7, Exposure 10 sec, Chopper Revolutions 3930)

APPENDIX B

SAMPLE CALCULATIONS

The following calculations were carried out for this work:

a) Flame air-fuel ratio

b) Adiabatic flame temperatures

c) Gas temperature corrections

d) Energy balance to estimate the percentage of aluminum consumed and mean particle diameter reduction

e) Aluminum particle mean speeds.

a) Flame Air-Fuel Ratio

Data: Air Pressure = 10.1 in Hg

Temperature = 77°F

Flowmeter Divisions = 7.0

Fuel Pressure = 1.9 in H_2O

Temperature = 78°F

Flowmeter Divisions = 3.5

Barometric pressure = 29.20 in Hg

The total volumetric flow of air and methane is read, in standard cubic feet per hour, from the flowmeter calibration curves included in Appendix C.

SCFH of Air = 53.5

SCFH of CH_4 = 1.9

This flow is corrected for pressure and temperature.

$$\dot{V}_{air} = 41.24 \text{ CFH}$$
$$\dot{V}_{CH_4} = 1.97 \text{ CFH}$$

The mass flow of air and methane is calculated using the equation of state

$$p\dot{V} = \dot{m}RT \tag{1}$$

so:

$$\dot{m}_{air} = 4.009 \text{ lb/h}$$
$$\dot{m}_{CH_4} = .142 \text{ lb/h}$$

The air-fuel ratio is given by:

$$\frac{A}{F} = \dot{m}_{air}/\dot{m}_{CH_4} \tag{2}$$

In this case:

$$A/F = 28.16 \text{ lb of air/lb of } CH_4$$

The combustion completion ratio is defined as:

$$\Phi = \frac{\text{Stochiometric air-fuel ratio}}{\text{Calculated air-fuel ratio}} \tag{3}$$

For methane the stochiometric air-fuel ratio is 17.13 lb of air/lb of CH_4. In this case $\Phi = 17.13/28.16 = 60.8\%$.

The gas velocity is calculated from the combined air and fuel

volumetric flow divided by the total burner disc area.

Porous disc diameter = 3.24 inches

Porous disc area = .0573 square feet

For this flame:

$$V = \frac{41.24 + 1.97}{3600 \times .0573} = .2096 \text{ ft/s} = 6.39 \text{ cm/s}$$

b) Adiabatic Flame Temperature

Complete combustion of the methane with no dissociation was considered to determine the maximum value of the adiabatic flame temperature.

Data: $A/F = 28.16$ g mole air/g mole CH_4

The following chemical equation is balanced.

$$CH_4 + aO_2 + 3.76\ aN_2 \rightarrow CO_2 + 2H_2O + 3.76\ aN_2 + (a-2)\ O_2 \qquad (4)$$

$$\frac{A}{F} = \frac{32a + 3.76\ a \times 28}{16} = 28.16$$

and

$$a = 3.28 \text{ moles of } O_2/\text{moles of } CH_4$$

The balance equation is:

$$CH_4 + 3.28\ O_2 + 12.34\ N_2 \rightarrow CO_2 + 2H_2O + 12.34\ N_2 + 1.28\ O_2 - Q$$

The heat of reaction is calculated using equation (5).

$$Q = \sum_p n_p \left\{h_f^o + (h_T - h_{537}^o)\right\}_p - \sum n_r \left\{h_f^o + (h_T - h_{537}^o)\right\}_r \qquad (5)$$

$$\frac{\text{Btu}}{\text{lb mole } CH_4}$$

For the adiabatic flame temperature Q = 0 so:

$$(h_T - h_{537}^o)_{CO_2} + 2(h_T - h_{537}^o)_{H_2O} + 12.34(h_T - h_{537}^o)_{N_2} + \qquad (6)$$

$$+ 1.282(h_T - h_{537}^o)_{O_2} = 345{,}169 \frac{\text{Btu}}{\text{lb mole } CH_4}$$

Equation (6) is used to determine the adiabatic flame temperature by a trial and error process. For this case with an air-fuel ratio of 28.16 the adiabatic flame temperature is 2904°R.

This temperature has been calculated for different air-fuel flames and is plotted in Figure C1 of Appendix C.

c) Gas Temperature Corrections for Radiation

The method used in this work for correcting gas temperatures measured by inserting a thermocouple was proposed by Fishenden in 1939 (27).

The main source of error in measuring the gas temperature is caused by the heat exchange by radiation between the thermocouple and the colder surrounding walls. The thermocouple will attain a temperature somewhere between that of the gas and the colder walls. The heat transferred by convection between the gas and the thermocouple is equated to the heat transferred by radiation between the thermocouple and the surrounding walls.

The calculations are first carried out neglecting gas radiation, and later a correcting factor is introduced to account for it. Equating the two modes of heat transfer we have:

$$h(t_g - t_c) = \alpha_R(t_c - t_w) \tag{7}$$

where

$$\frac{h \cdot d}{k} = f\left(\frac{vd\rho}{\mu}\right) \tag{8}$$

Equation (6) is reduced to:

$$\frac{t_g - t_c}{t_c - t_w} = NdE \tag{9}$$

N depends on the absolute mean temperature between the measured gas temperature and that of the wall, the gas thermal conductivity, and Reynolds number. Fishenden has calculated N for different values of the mean temperature using appropriate values for ρ, μ, and k for air taken at the mean temperature. The values of ρ, μ, and k for CO_2, CO, N_2, O_2, and water vapor are sufficiently close to those of air. The error introduced is within the limits for which the whole calculation is liable. The value of N is plotted using the product of the gas velocity times the thermocouple diameter as abscissa (27).

The calculations will be carried out for the temperature measured in the $\frac{1}{16}$ inch plane of a flame with $\Phi = .608$.

Data: Measured temperature $t_c = 1637^\circ F$

Wall temperature $t_w = 230^\circ F$

Thermocouple diameter d = .013 inch

Gas velocity V = .210 ft/s

Thermocouple emissivity E = .05

Gas emissivity e = .10

V X d = .0034 ft/s in

Mean temperature $t_m = 934^\circ F$

The value of N is read from Fishenden's graph; for this case N = 82.

The gas temperature is calculated from equation (9). Thus

$$t_g = 1724^\circ F$$

The modification to the calculation, to allow for gas radiation, is extremely complicated and can be done only approximately. Equation (9) is multiplied by a correction factor:

$$\frac{t_{g_R} - t_c}{t_c - t_w} = NdE\ (1-x) \tag{10}$$

where

$$x = \frac{T_g^4 - T_w^4}{T_c^4 - T_w^4}\ e \tag{11}$$

The corrected gas temperature is:

$$t_{g_R} = 1709^\circ F$$

A program was written to calculate the correct gas temperature using a 300 Series Wang Calculator.

d) Estimating Aluminum Particle Reaction

The assumptions mentioned in Chapter IV were used to carry out these calculations. An energy balance was performed in the reaction zone to estimate the amount of aluminum consumed and average particle diameter reduction.

Data: Combustion completion ratio $\Phi = .914$

Mass flow of nitrogen $\dot{m}_{N_2} = 475.8$ g/h

Mass flow of aluminum $\dot{m}_{Al} = 9.83$ g/h

Mass flow of methane $\dot{m}_{CH_4} = 64.4$ g/h

Wall emissivity $\varepsilon_w = 0.9$

Particle mean diameter $D = 50$ μm

The control volume used has an upper boundary at the $\frac{1}{8}$ inch plane.

Table 3. Mean Temperatures for Estimating Aluminum Particle Reaction. $\Phi = .914$, $H = \frac{1}{8}$ inch

Nitrogen-Jet °K		Nitrogen-Particle Jet °K	
Edge	Center	Edge	Center
1156	382	1231	1012

1. Heat of Reaction for the Flame with the Opposed Nitrogen Jet

The chemical equation to be balanced is:

$$CH_4 + aO_2 + 3.76\ aN_2 + 4.221\ N_2 \rightarrow \qquad (12)$$

Jet at 982°K

$$CO_2 + 2H_2O + (a-2)O_2 + (3.76\ a + 4.221)\ N_2 - Q$$

at 1156°K

The heat of reaction is calculated using equation (5)

so: $$Q = -106{,}809 \text{ cal/g mole } CH_4$$

The combined conduction and radiation losses must be calculated. The radiation losses are given by the equation

$$g_R = A_w \frac{\epsilon_w + 1}{2} \sigma(\epsilon_g T_g^4 - \alpha_g T_w^4) \tag{13}$$

The gas emissivity can be calculated using the method outlined by Hottel and Sarafim (30)

so: $$\epsilon_g = .09$$

The gas absorptivity is given by equation

$$\alpha_g = \left(\frac{T_g}{T_w}\right)^{\frac{1}{2}} \epsilon_g \tag{14}$$

so $$\alpha_a = .161$$

The wall area considered is a strip of the glass chimney $\frac{1}{8}$ inch high. Introducing these data into equation (13), the radiation losses are found to be 183.5 Btu/hr. The combined losses are 283.5 Btu/hr assuming 100 Btu/hr lost by conduction. The losses are reduced to cal/g mole CH_4 using the total mass flow of gases and the mean molecular weight of the products. The total losses are:

$$g = 4044 \text{ cal/g mole } CH_4$$

and the net heat of reaction is

$$Q = -102{,}765 \text{ cal/g mole } CH_4$$

2. Heat of Reaction for the Flame with the Opposed Nitrogen-Aluminum Particle Jet

The aluminum is assumed to undergo a heating process without any chemical reaction.

So:

$$CH_4 + 2.184\ O_2 + 8.213\ N_2 + 4.221\ N_2 + .0905\ Al \rightarrow \quad (15)$$

at 298°K Jet at 1012°K

$$\rightarrow CO_2 + 2H_2O + 12.43\ N_2 + .184\ O_2 + .0905\ Al - Q$$

at 1231°K

The heat of reaction calculated in this case is - 97,424 cal/g mole CH_4 while the losses are 4405 cal/g mole CH_4. The net heat of reaction is:

$$Q = -93{,}019 \text{ cal/g mole } CH_4$$

The difference between the heat of reaction calculated in 1 and in 2 is due to heat released by the chemical reaction of aluminum.

so
$$\Delta Q_{1-2} = b\ h^{o}_{f_{Al_2O_3}} \quad (16)$$

$$.0905\ Al + .184\ O_2 \rightarrow bAl_2O_3 + cAl + dO_2 \quad (17)$$

so $b = .0243$

$c = .0419$

$d = .148$

The total aluminum consumed in this case is 5.28 g/h; this is equivalent to a 53.69% reduction in volume. The new mean particle diameter can be calculated from

$$D = 50 \left(\frac{53.69}{100}\right)^{\frac{1}{3}} \tag{18}$$

assuming that the particles have an initial diameter of 50 μm.

so $D = 38.68$ μm.

e) Aluminum Particle Mean Speeds

The particle mean speeds were calculated directly from the photographic records.

Data: Combustion completion ratio $\Phi = .835$

Mass flow of nitrogen $\dot{m}_{N_2} = .412$ lb/h

Chopper revolutions $n = 3145$ rpm

Photographic scale $1'' = 1.19''$

Measured distance between two segments of a trace = .240 inch

The true distance between two segments of a trace is:

$$s = .240 \times 1.19 = .286 \text{ inch}$$

The time elapsed between segments of the particle traces is calculated from the light chopper revolutions:

$$t = \frac{3 \times 10^4}{n} \quad \text{msec} \tag{19}$$

the particle mean speed is:

$$v_p = \frac{.286}{9.5} \times 10^3 = 29.95 \text{ in/s}$$

$$= 76.5 \text{ cm/s}$$

APPENDIX C

ADIABATIC FLAME TEMPERATURE, FLAME FLAMABILITY LIMITS, AND FLOWMETER CALIBRATION CURVES

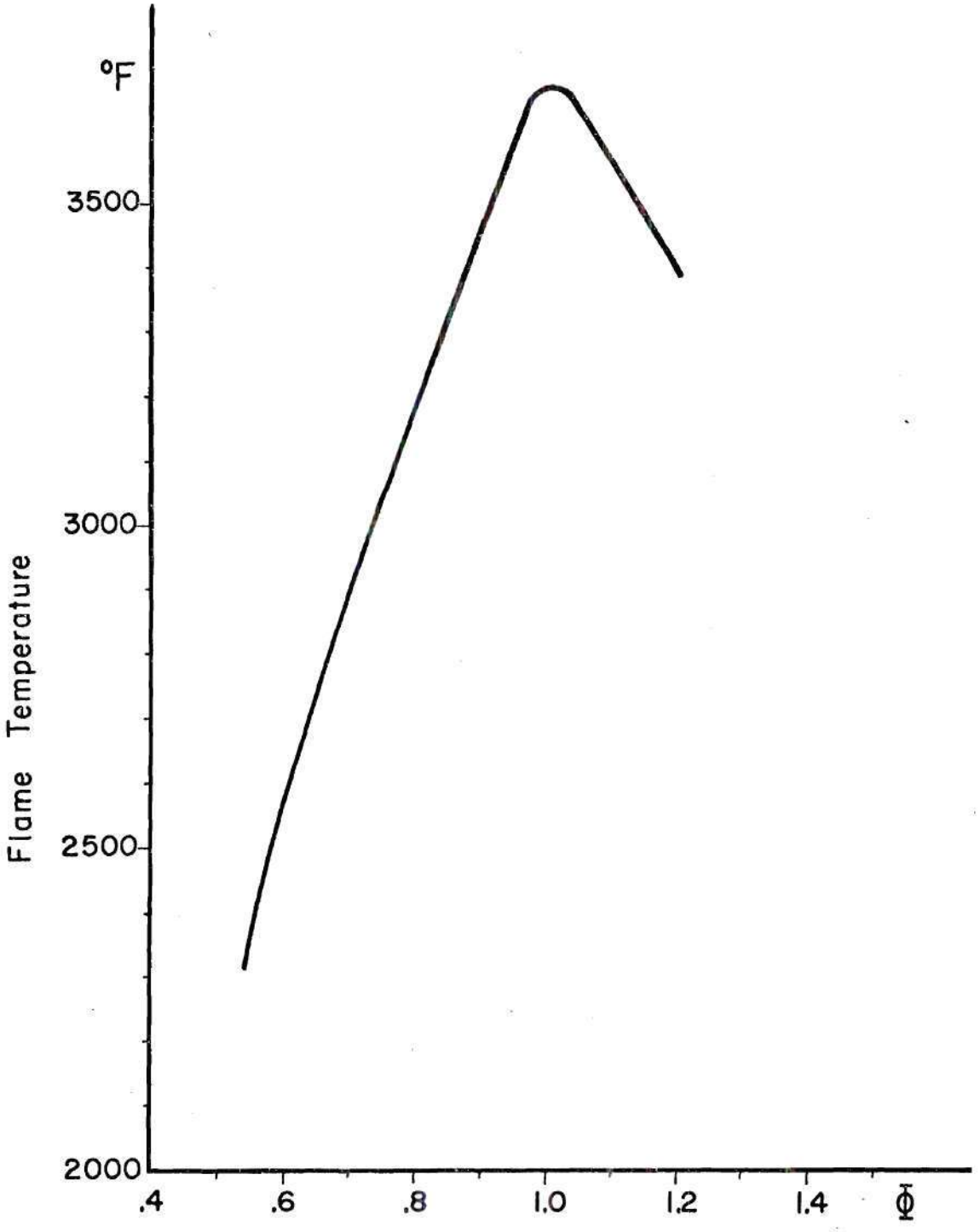

Figure C1. Adiabatic Flame Temperature.

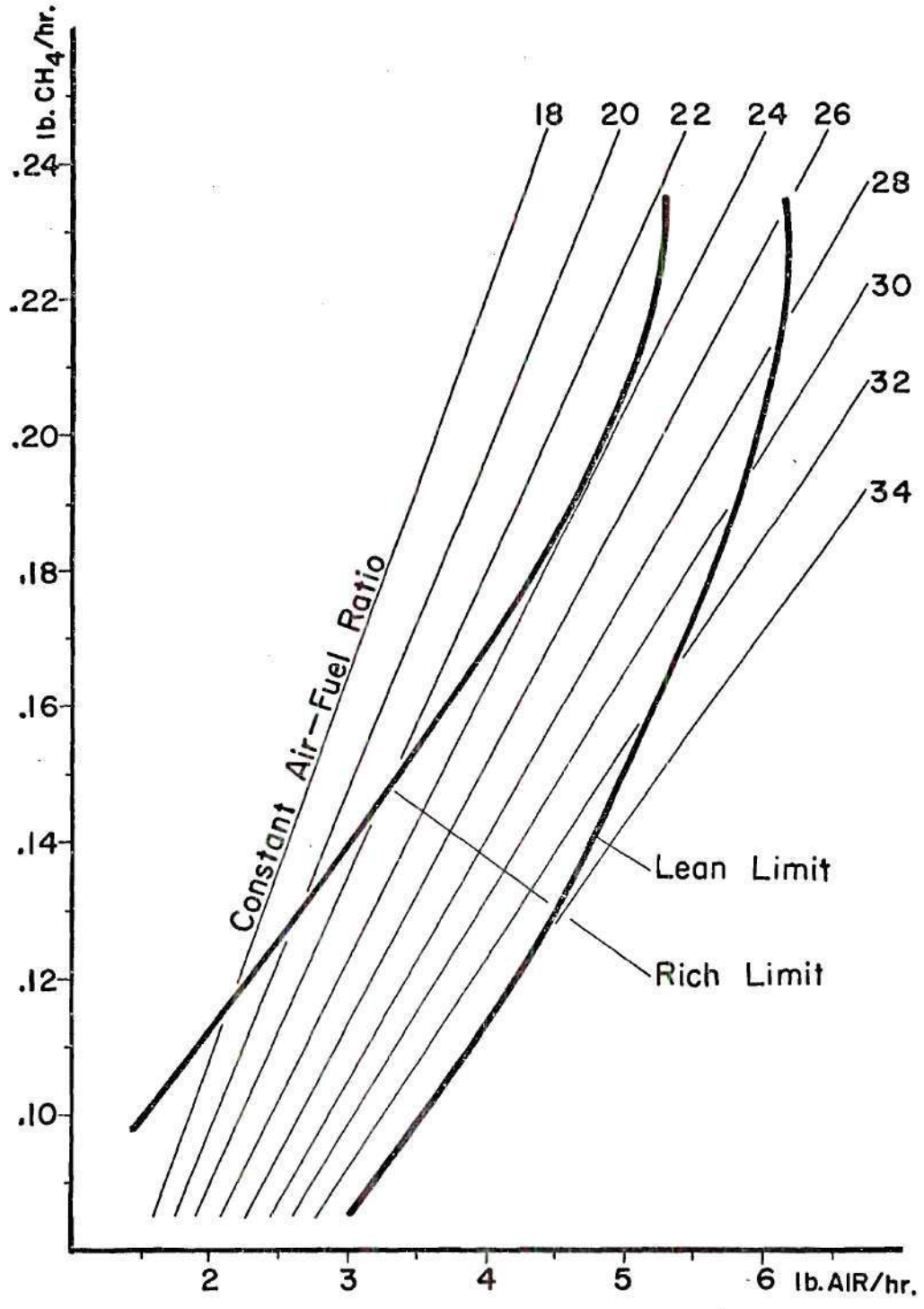

Figure C2. Stable Flat Flame Limits.

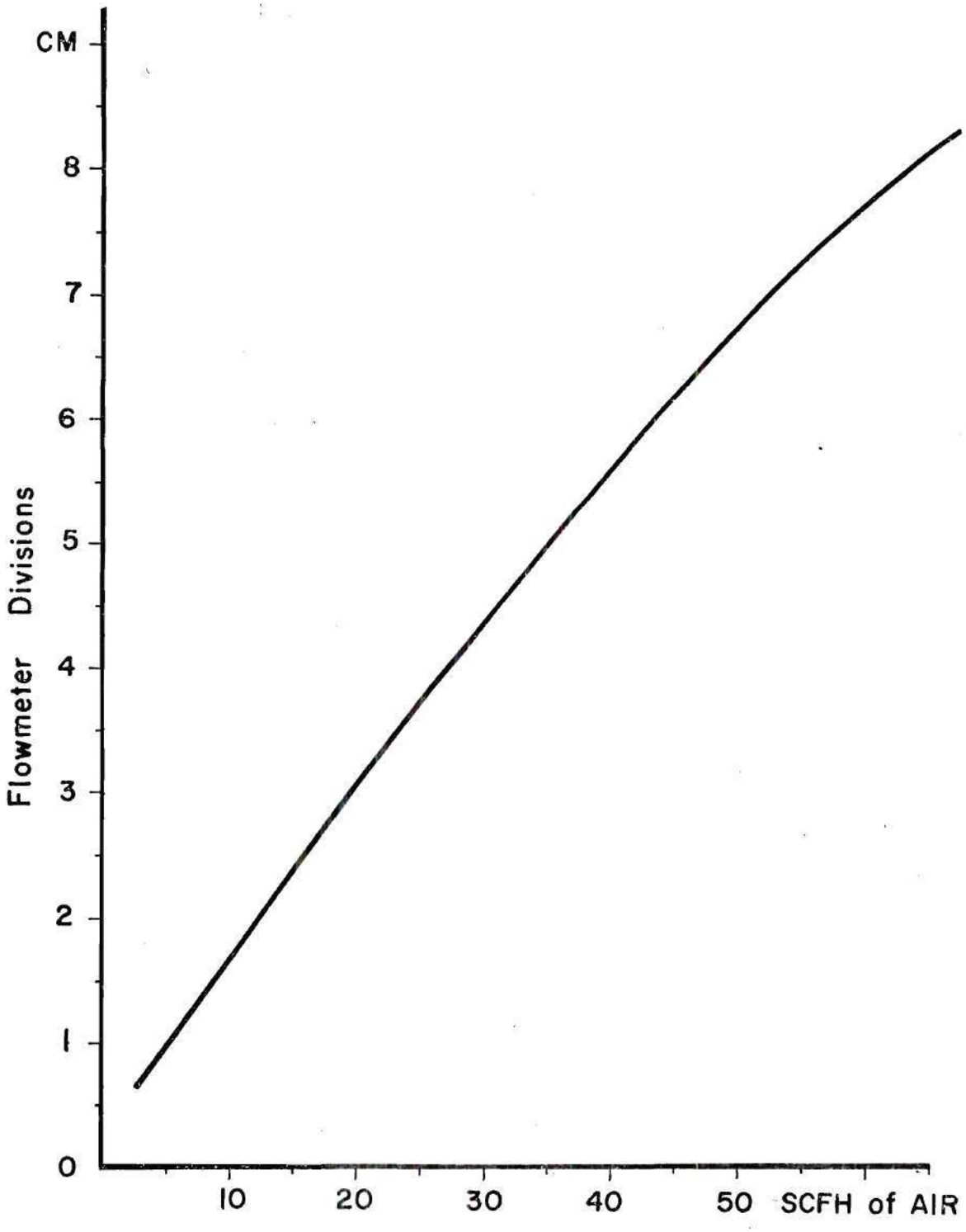

Figure C3. Calibration Curve for AIR Flowmeter.

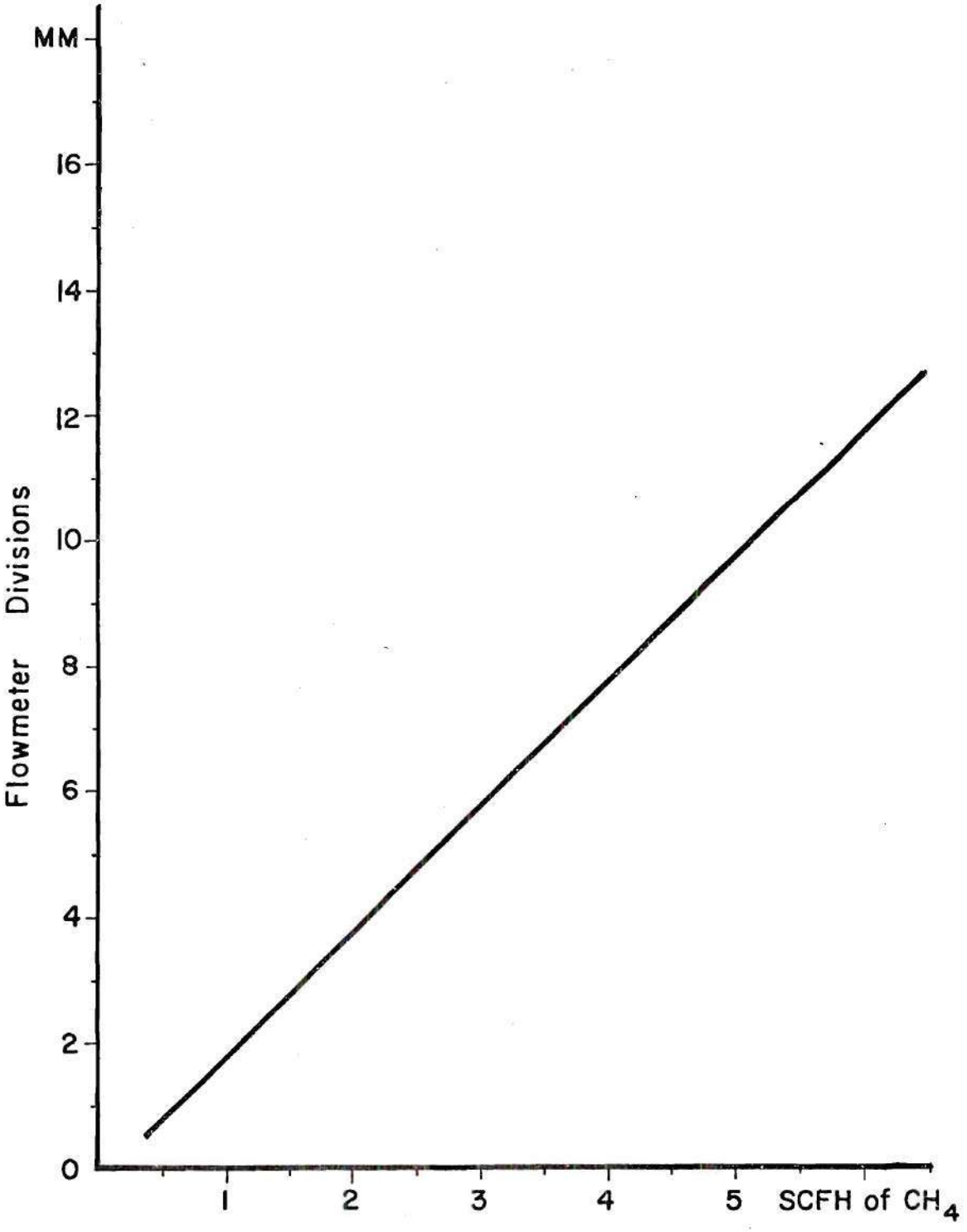

Figure C4. Calibration Curve for CH_4 Flowmeter.

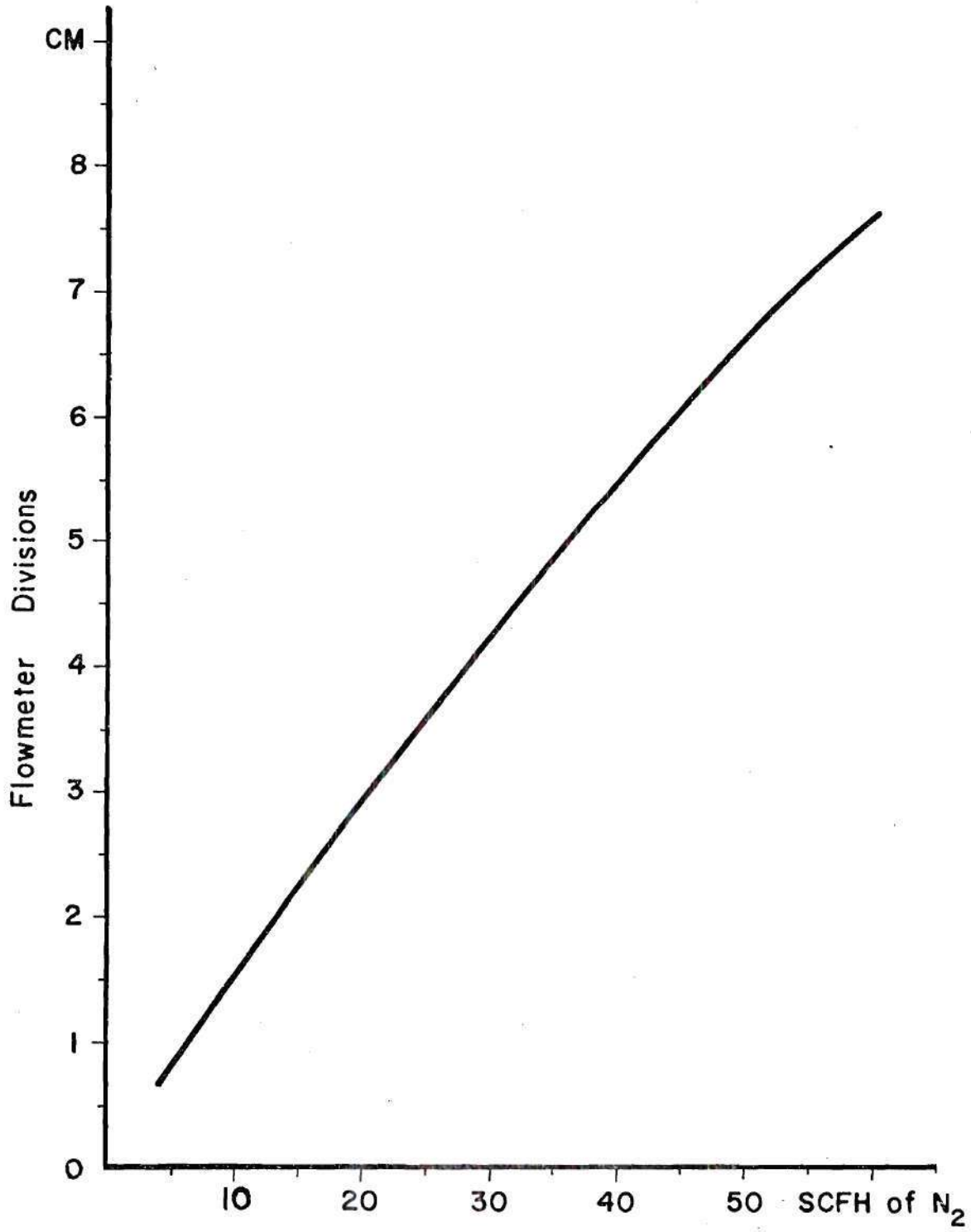

Figure C5. Calibration Curve for Total N_2 Flowmeter.

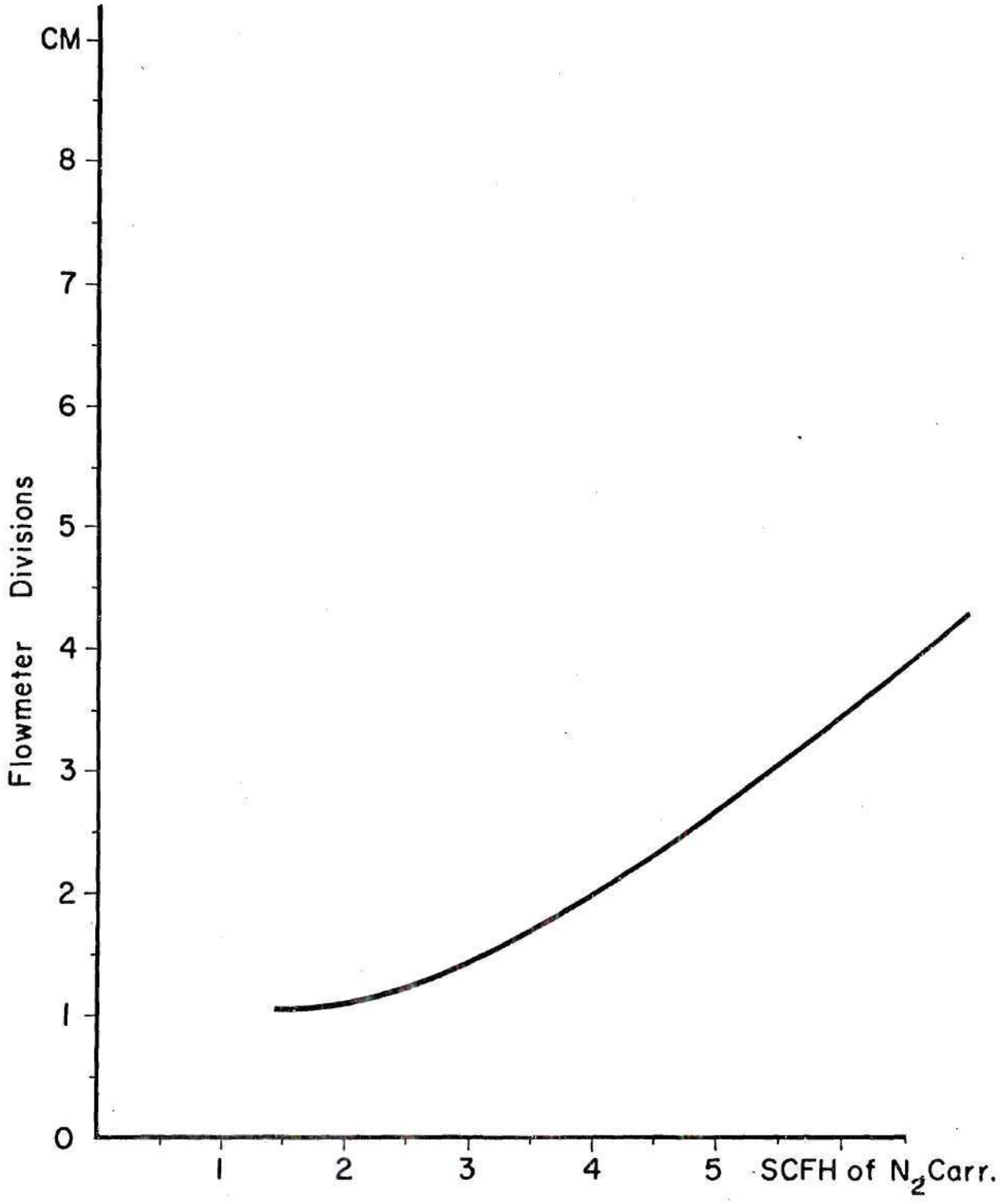

Figure C6. Calibration Curve for Carrier N_2 Flowmeter.

LITERATURE CITED

1. A. Shakill, "Design and Preliminary Testing of a Pre-mixed Flat Flame Burner Incorporating an Opposed Gas-Particle Jet," M.S. Thesis, March 1970, Georgia Institute of Technology.

2. R. Bartlett, Combustion and Flames, 8, 341 (1964).

3. R. Friedman and A. Macek, "Combustion Studies of Single Aluminum Particles," Ninth Symposium (International) on Combustion, The Williams & Wilkins Company, Baltimore, 703 (1963).

4. J. Prentice, "On Combustion of Single Aluminum Particles," Combustion and Flames, 9, 208 (1965).

5. R. Bartlett, J. Ong, and W. Fassell, "Estimating Aluminum Particle Combustion Kinetics," Combustion and Flames, 7, 227 (1963).

6. G. Bahn, "On Pyrophoricity of Metals and of Fine Metal Powders in Particular," Pyrodynamics, 3, 29 (1965).

7. T. Brgustowski and I. Glassman, "Vapor Phase Diffusion Flames in the Combustion of Aluminum and Beryllium I," American Institute of Aeronautics and Astronautics Journal, 15, 75 (1964).

8. T. Brzustowski and I. Glassman, "Vapor Phase Diffusion Flames in the Combustion of Aluminum and Beryllium II," American Institute of Aeronautics and Astronautics, 15, 117 (1964).

9. A. Davis, "Solid Propellants, the Combustion of Particles of Metal Ingredients," Combustion and Flames, 7, 359 (1963).

10. I. Glassman, "Combustion of Metals Physical Considerations," American Rocket Society, 1, 253 (1960).

11. A. Gordon, "Combustion Characteristics of Metal Particles," Eleventh Symposium (International) on Combustion, The Reinhold Publishing Corp., New York, 215 (1967).

12. D. Kuehl, "The Ignition and Combustion of Small Diameter Aluminum Wires," Pyrodynamics, 3, 65 (1965).

13. D. Kuehl, "Ignition and Combustion of Aluminum and Beryllium," American Institute of Aeronautics and Astronautics Journal, 3, 2239 (1965).

LITERATURE CITED (Continued)

14. A. Macek and J. Semple, "Experimental Burning Rates and Combustion Mechanism of Single Beryllium Particles," Twelfth Symposium (International) on Combustion, The Reinhold Publishing Corp., New York, 71 (1969).

15. A. Macek, "Fundamentals of Combustion of Single Aluminum and Beryllium Particles," Eleventh Symposium (International) on Combustion, The Reinhold Publishing Corp., New York, 203 (1967).

16. A. Macek and R. Friedman, "Techniques for the Study of Combustion of Beryllium and Aluminum," American Institute of Aeronautics and Astronautics Journal, 3, 16 (1965).

17. H. Christensen and R. Knipe, "Survey of Aluminum Particle Combustion," Pyrodynamics, 3, 91 (1965).

18. G. Markestein, "Heterogeneous Reaction in Metal Combustion," Eleventh Symposium (International) on Combustion, The Reinhold Publishing Corp., New York, 219 (1967).

19. V. Yumlu, "Temperature of Flames on Porous Burners," Combustion and Flames, 10, 147 (1966).

20. W. Bowen, "Temperature Measuring Instruments," Journal Institute of Fuel, 12, 575 (1939).

21. R. Tourin, "Spectroscopic Gas Temperature Measurements," J. M. Beer Editor, Elsevier (1966).

22. P. Loomis and C. Periott, "Measurements of the Temperature of Stationary Flames," Journal Analytical Chemistry, 30, 1004 (1928).

23. G. Dixon and B. Lewis, "Method for the Measurement of the Temperature Distribution in the Inner Cone of a Bunsen Flame," Transactions Faraday Society, 47, 1106 (1951).

24. H. Kreisinger, "Radiation Error in Measuring Temperature of Gases," Transactions American Society of Mechanical Engineers, 39, 107 (1917).

25. B. Larsen, G. Sidall, and K. Hendlhoffer, "A Modified Aspirating Thermocouple for Gas Temperature," Journal Institute of Fuel, 12, 555 (1939).

26. G. Mitchell and J. Lobdell, "Resistance Thermometer Measurements in a Low Pressure Flame," Journal Institute of Fuel, 12, 285 (1964).

LITERATURE CITED (Concluded)

27. M. Fishenden and O. Sanders, "The Error in Gas Temperature Measurements and Their Calculation," Journal Institute of Fuel, 12, 55 (1964).

28. C. Robinson, "Radiation Effects in Thermometry," Industry Engineering and Chemistry, 13, 820 (1921).

29. M. Jakob, "Heat Transfer," John Wiley and Sons, Inc., New York, Vol. II, 120 (1967).

30. H. Hottel and F. Sarafim, "Radiation Transfer," McGraw-Hill Book Company, New York, 277 (1967).

OTHER REFERENCES

Beal, J. and Brown, W., "Oxidation and Explosion of Drops of Molten Zirconium Metal," Pyrodynamics, 3, 135 (1965).

Bielder, W., "Studies in a New Type of Flat Flame Burner," Jet Propulsion Journal, 27, 1257 (1957).

Brandmaier, H., "Particulate Cloud," H. Green and W. Lane, Van Nostrand, Princeton, New Jersey, 383 (1964).

Brzustowski, T. and Glassman, I., "Spectroscopic Investigation of Metal Combustion," AIAA Journal, 15, 41 (1964).

Coffin, K. and Bwkan, R., "A General System for Calculating Burning Rates of Particles and Drops and Comparison of Calculated Rates for Carbon, Boron, Magnesium and Iso-octane," NACA TN 3929 (1957).

Da Rosa, A., "A Comparison of Relative Values of Fuel," American Rocket Society Journal, 14, 4 (1945).

Dieke, G., "High Gas Temperature," Temperature Its Measurement and Control in Science and Industry, 2, 19 (1965).

Dixon, G. and Lewis, B., "Flame Structure Studies," Eighth Symposium (International) on Combustion, The Reinhold Publishing Corp., New York, 448 (1962).

Dixon, G. and Lewis, B., "Temperature Distribution in Flame Reaction Zones," Fourth Symposium (International) on Combustion, The Williams and Wilkins Company, Baltimore, 263 (1953).

Drew, C. and Gordon, A., "Study of Quenched Aluminum Particle Combustion," AIAA Journal, 17, 39 (1964).

Edhigo, R., "A Study on the Radiation of Luminous Flames," Eleventh Symposium (International) on Combustion, The Reinhold Publishing Corp., New York, 381 (1967).

Fisher, G., "A Study of the Aerodynamic Properties of a Lifted Flat Flame," Combustion and Flame, 12, 333 (1967).

Friedman, R., "Measurements of the Temperature Profile in a Laminar Flame," Fourth Symposium (International) on Combustion, The Williams and Wilkins Company, Baltimore, 259 (1953).

OTHER REFERENCES (Concluded)

Fustrom, R., "Flame Structure," McGraw-Hill Book Company, New York (1965).

Hottel, H., "Determination of the True Temperature and Total Radiation from Luminous Gas Flames," Industry Engineering and Chemistry, 4, 196 (1932).

Mellor, M. and Glassman, I., "A Physical Criterion for Metal Ignition," Pyrodynamics, 3, 43 (1965).

Nelson, L., "Combustion of Metal Droplet Ignited by Flash Heating," Eleventh Symposium (International) on Combustion, The Reinhold Publishing Corp., New York, 409 (1967).

Prentice, J. and Drew, C., "Preliminary Studies of High Speed Photography of Aluminum Particles in Flames," Pyrodynamics, 3, 81 (1965).

Reynolds, W., "Investigation of Ignition Temperatures of Solid Metals," NASA TN-D-182 (1959).

Rhein, R., "The Combustion of Powdered Metal in N_2 and CO_2," Pyrodynamics, 3, 161 (1965).